

Article

Enhancement of the Luminescent Efficiency in Carbene-Au(I)-Aryl Complexes by the Restriction of Renner–Teller Distortion and Bond Rotation

Tian-yi Li, Daniel Sylvinson Muthiah Ravinson, Ralf Haiges, Peter I. Djurovich, and Mark E. Thompson

J. Am. Chem. Soc., **Just Accepted Manuscript** • DOI: 10.1021/jacs.9b13755 • Publication Date (Web): 02 Mar 2020

Downloaded from pubs.acs.org on March 2, 2020

Just Accepted

“Just Accepted” manuscripts have been peer-reviewed and accepted for publication. They are posted online prior to technical editing, formatting for publication and author proofing. The American Chemical Society provides “Just Accepted” as a service to the research community to expedite the dissemination of scientific material as soon as possible after acceptance. “Just Accepted” manuscripts appear in full in PDF format accompanied by an HTML abstract. “Just Accepted” manuscripts have been fully peer reviewed, but should not be considered the official version of record. They are citable by the Digital Object Identifier (DOI®). “Just Accepted” is an optional service offered to authors. Therefore, the “Just Accepted” Web site may not include all articles that will be published in the journal. After a manuscript is technically edited and formatted, it will be removed from the “Just Accepted” Web site and published as an ASAP article. Note that technical editing may introduce minor changes to the manuscript text and/or graphics which could affect content, and all legal disclaimers and ethical guidelines that apply to the journal pertain. ACS cannot be held responsible for errors or consequences arising from the use of information contained in these “Just Accepted” manuscripts.

Enhancement of the Luminescent Efficiency in Carbene-Au^(I)-Aryl Complexes by the Restriction of Renner–Teller Distortion and Bond Rotation

Tian-yi Li, Daniel Sylvinson Muthiah Ravinson, Ralf Haiges, Peter I. Djurovich, Mark E. Thompson*

Department of Chemistry, University of Southern California, Los Angeles, CA 90089, United States

Abstract

A series of (carbene)Au^(I)(aryl) complexes are reported. The nature of the lowest excited state in these complexes changes character from metal-to-ligand charge transfer (MLCT) to interligand charge transfer (ICT) with increasing electron donating strength of the aryl ligand. Complexes that have an MLCT lowest excited state undergo a Renner–Teller bending distortion upon excitation. Such a distortion leads to a large rate for nonradiative decay, on the order of 10^8 s⁻¹. Renner–Teller based nonradiative decay does not occur in chromophores with an ICT emissive state. Introducing a julolidine moiety and ortho-methyl substituents to the aryl group makes the molecule rigid and hinders the rotation along Au–C_{aryl} coordinate bond. Consequently, nonradiative decay rates of these ICT emitters are decreased and become lower than the radiative decay rate constants ($k_r = 10^5$ s⁻¹). Thus, high luminescence efficiencies ($\Phi_{PL} = 0.61$ and 0.77) along with short lifetimes ($\tau < 2$ μ s) are obtained for yellow and green emitters, respectively. Thermally assisted delayed fluorescence behavior is observed owing to the small exchange energy ($\Delta E_{ST} < 1600$ cm⁻¹) in these emitters.

Introduction

Linear, two coordinate, neutral, d¹⁰ coinage metal (Cu, Ag and Au) complexes with a general formula (carbene)M^(I)(amide) have emerged as promising luminescent materials.¹ These complexes have high photoluminescence quantum yields (Φ_{PL}) and short luminescent decay lifetimes (τ). By judicious choice of the carbene ligand, metal atom and amide, highly efficient luminescence ($\Phi_{PL} \sim 1.0$) can be obtained with

1
2
3 fast radiative decay ($\tau < 1 \mu\text{s}$), values comparable to properties of phosphorescent complexes using noble
4 metals (Ir and Pt).^{1a-c} The origin of their distinguished photophysical properties is the emissive
5 amide-to-carbene interligand charge transfer (ICT) state, which emits via thermally assisted delayed
6 fluorescence (TADF). Since the highest occupied molecular orbital (HOMO) localized on the π electron
7 donating amide and the lowest unoccupied molecular orbital (LUMO) on carbene acceptor are well
8 separated ($C_{\text{carbene}} \cdots N_{\text{amid}}$ distance is $\sim 4 \text{ \AA}$), the energy gap between the S_1 and T_1 states (ΔE_{ST}) is small.
9
10 Therefore, in conjunction with rapid intersystem crossing (ISC) induced by the heavy metal atom, fast rates
11 of $T_1 \rightarrow S_1$ ISC up to 10^8 - 10^9 s^{-1} are possible.^{1a} TADF emitters without metal ions show bimodal emission
12 decay, with both prompt ($\tau < 100 \text{ ns}$) and delayed emission ($\tau > 10 \mu\text{s}$) signatures, where the relative
13 intensity of the former is largely determined by the slow ISC rate and the latter by size of ΔE_{ST} .² In contrast,
14 the (carbene)M(amide) complexes present mono-exponential emissive decays on the 0.5 – $2 \mu\text{s}$ timescale
15 (neglecting the 20 – 200 ps component associated with ISC).³
16
17
18
19
20
21
22
23
24
25
26
27
28
29

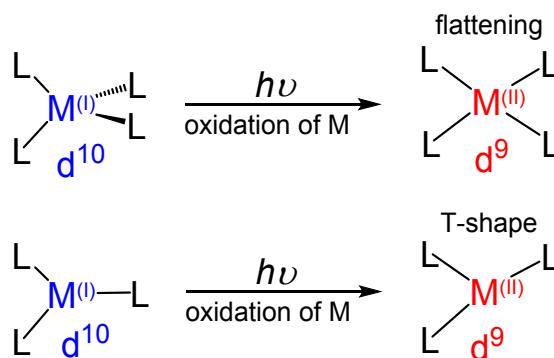
30 Many recent investigations of luminescent Au complexes are focused on square-planar d^8 Au^{III} with
31 bidentate⁴ or pincer tridentate ligands.⁵ Several reports have also recently appeared that describe Au^{III}
32 complexes which display luminescent properties associated with TADF emission.⁶ However, due to the
33 unfilled d orbital in Au^{III} complexes, these complexes can undergo nonradiative decay through low-lying
34 d-d states. Such a nonradiative decay route can be avoided in two-coordinate Au^{I} complexes with a filled
35 d^{10} configuration. Several reports of emissive two-coordinate $\text{Au}(\text{aryl})$ complexes have also appeared.⁷
36
37 Previous studies on these derivatives have described materials that luminesce from metal-metal states
38 induced by aurophilic interactions or from intraligand π - π^* states;⁸ however, there do not appear to be any
39 reports of mononuclear, two-coordinate Au complexes where emission occurs from metal-to-ligand charge
40 transfer (MLCT) states.⁹ Here we investigate changing the donor ligands in the previous reported
41 (carbene)Au(amide) complexes to aryl ligands, establishing a new series of luminescent two-coordinate
42 Au^{I} chromophores with a general structure of (carbene)Au(aryl).^{7b, 10}
43
44
45
46
47
48
49
50
51
52
53
54
55
56
57
58
59
60

Most previously reported d^{10} coinage metal emitters have three- or four-coordinate geometry.¹¹ Upon photoexcitation to the MLCT state, the metal center is transiently oxidized to a d^9 configuration. Consequently, these compounds suffer from Jahn–Teller distortion as shown in Figure 1. This process involves breaking the degeneracy of the orbitals due to asymmetric occupancy of the d -orbitals in the d^9 configuration. To minimize the overall molecular energy, four coordinate species with tetrahedral ground state undergo a flattening distortion after

photoexcitation,¹² whereas the trigonal planar, three coordinate complexes undergo T-shaped structural reorganization in the excited state.¹³ In such cases, the nonradiative decay rate is sufficiently fast to severely limit luminescence in fluid environments, owing to the enhanced Franck–Condon factors between vibronic states of the excited and ground electronic state.¹⁴ Similarly, when the MLCT state is the lowest excited state, linear d^{10} coinage complexes can also nonradiatively decay through a geometric distortion, but in this case, the deformation involves bending,^{9d, 15} referred to as the Renner–Teller effect (Figure 1c).¹⁶ The driving force for such distortion comes from stabilization of the excited state caused by orbital mixing in the new geometry as a result of high-order vibrational and electronic coupling in the open-shell system.¹⁷

To preclude significant nonradiative energy loss induced by Renner–Teller distortion in two coordinate complexes, the lowest excited state (the emissive state) must avoid a change in valence of the metal ion, *i.e.* not be an MLCT state.¹⁵ This energetic condition was met in our previous (carbene) $M^{(I)}$ (amide) compounds by virtue of using electrophilic diamidocarbene (DAC) and monoamido-aminocarbene (MAC) ligands as acceptors and amides as a strong electron donors.^{1a, 1c} Similarly, by employing the same DAC

Jahn-Teller distortion



Renner-Teller distortion

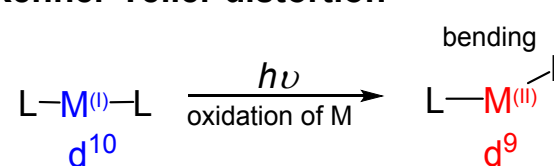


Figure 1. Schematically illustrations of molecular distortion mechanisms for d^{10} coinage metal complexes upon excitation to a MLCT excited state.

1
2
3 and MAC ligands, and by adding electron donating substituents to the energetically low-lying π orbital of
4 the phenyl ligand to destabilize the energy level of the HOMO, a (carbene)Au(aryl) complex should have
5 a lowest emissive state with ICT character. To validate this hypothesis, a series of (DAC)Au(aryl) and
6 (MAC)Au(aryl) complexes were synthesized where substituents with increasing electron donor strength on
7 the aryl ligand were used to destabilize the energy level of the aryl π orbital, thus, shifting the HOMO
8 energy away from the Au center and onto the aryl ligand. On the basis of theoretical calculations and
9 photophysical studies, we conclude that Renner–Teller distortions occur in complexes with MLCT excited
10 states, but not in compounds that have an ICT lowest excited state. Such a distortion leads to a significant
11 increase in nonradiative decay rate, which can enhance nonradiative decay and make the chromophore
12 poorly or non-emissive. We also investigate the role of aryl- and amide-group rotation in nonradiative decay
13 of these complexes. We find that restricting rotation in addition to eliminating Renner–Teller distortion
14 leads to a marked increase in the luminescence efficiency (Φ_{PL} increasing from $< 10^{-3}$ to 0.77), owing to a
15 decrease in nonradiative decay (from $>10^8$ to *ca.* $5 \times 10^4 \text{ s}^{-1}$).
16
17
18
19
20
21
22
23
24
25
26
27
28
29
30

31 Experimental Section

32
33
34 **Synthesis and characterization.** All the boronic acid except 4-dimethylamino-2,6-dimethyl boronic acid
35 are purchased from commercial sources and used without further purification.
36 4-dimethylamino-2,6-dimethyl boronic acid and 3,5-dimethyl-4-julolidine boronic acid pinacol ester were
37 synthesized using modified methods according to the previous reports, synthetic details are provided in the
38 electronic supporting information (ESI).¹⁸ The carbene ligands were synthesized according to the reported
39 methods.^{1c} All the reactions are carried out using standard Schleck techniques, and the purification of the
40 products are carried out under air. All the solvents were used as received from commercial sources except
41 where individually mentioned. ¹H NMR and ¹³C NMR spectra were recorded on a Varian Mercury 400
42 instrument. Elemental analyses were performed using a Thermo Scientific FlashSmart CHNS elemental
43 analyzer.
44
45
46
47
48
49
50
51
52
53
54
55
56
57
58
59
60

1
2
3 *General synthesis of (carbene)Au(aryl) from boronic acid (Method A):* In an oven-dried glass dram vial,
4 the (carbene)AuCl precursor (50 mg) and KOH (1.5 equiv) were stirred in a mixed solvent of benzene and
5 toluene (2 ml, 1:1 v/v) for 2 h at room temperature while covered with aluminum foil. Then, the
6 corresponding boronic acid (1.5 equiv) was added in one portion and the mixture was kept stirring at room
7 temperature. Upon complete conversion of the precursor (monitored by ¹H NMR), excess CH₂Cl₂ (20 ml)
8 was added and the suspension was filtered through a pad of Celite, providing a clear filtrate. After removal
9 of solvents under vacuum, a small amount of CH₂Cl₂ was added to dissolve the raw solid and pentane was
10 added to precipitate the desired product as a microcrystalline powder.
11
12
13
14
15
16
17
18
19

20
21 *General synthesis of (carbene)Au(aryl) from boronic acid pinacol ester (Method B):* In an oven-dried glass
22 dram vial, the (carbene)AuCl precursor (50 mg), the corresponding boronic acid ester (1.2 equiv) and KOH
23 (1.5 equiv) were suspended in a mixed solvent of benzene and toluene (2 ml, 1:1 v/v). The mixture was
24 stirred at room temperature for 12 h. Upon complete conversion of the precursor (monitored by ¹H NMR),
25 excess CH₂Cl₂ (20 ml) was added and the suspension was filtered through a pad of Celite, providing a clear
26 filtrate. After removal of solvents under vacuum, a small amount of CH₂Cl₂ was added to dissolve the raw
27 solid and pentane was added to precipitate the desired products as a microcrystalline powder.
28
29
30
31
32
33
34
35

36 *(DAC)Au^(I)(phenyl) (1a):* Method A, dark yellow microcrystalline powder, yield 44 mg (83%). ¹H NMR
37 (400 MHz, acetone) δ 7.54 (t, *J* = 7.8 Hz, 2H, *p*-ArH(dipp)), 7.39 (d, *J* = 7.8 Hz, 4H, *m*-ArH(dipp)), 6.82
38 – 6.73 (m, 2H, *m*-ArH), 6.65 (ddt, *J* = 8.0, 6.8, 1.5 Hz, 1H, *p*-ArH), 6.53 – 6.48 (m, 2H, *o*-ArH), 3.04 (sept,
39 *J* = 6.7 Hz, 4H, CH(CH₃)₂), 1.87 (s, 6H, C(CH₃)₂), 1.39 (d, *J* = 6.8 Hz, 12H, CH(CH₃)₂), 1.19 (d, *J* = 6.8 Hz,
40 12H, CH(CH₃)₂). ¹³C NMR (101 MHz, acetone) δ 227.57 (NCN), 172.65 (C=O), 166.18 (ipso-Au-Ar),
41 145.54 (ipso-N-Ar(dipp)), 140.25 (*o*-Ar), 134.87 (*o*-Ar(dipp)), 130.09 (*p*-Ar(dipp)), 125.96 (*p*-Ar), 124.44
42 (*m*-Ar), 124.30 (*m*-Ar(dipp)), 51.43 (C(CH₃)₂), 28.78 (CH(CH₃)₂), 24.38 (C(CH₃)₂), 23.63 (CH(CH₃)₂),
43 23.13 (CH(CH₃)₂). Elemental analysis calculated for C₃₆H₄₅AuN₂O₂: C, 58.85; H, 6.17; N, 3.81. found: C,
44 58.46; H, 6.57; N, 4.09.
45
46
47
48
49
50
51
52
53
54
55
56
57
58
59
60

(DAC)Au^(I)(4-carbazolylphenyl) (**1b**): Method A, bright yellow microcrystalline powder, yield 51 mg (78%). ¹H NMR (400 MHz, acetone) δ 8.14 (dt, *J* = 7.6, 1.0 Hz, 2H, CH⁴(Cz)), 7.58 (t, *J* = 7.8 Hz, 2H, *p*-ArH(dipp)), 7.45 (d, *J* = 7.7 Hz, 4H, *m*-ArH(dipp)), 7.34 (ddd, *J* = 8.3, 7.1, 1.2 Hz, 2H, CH²(Cz)), 7.24 (dt, *J* = 8.3, 0.8 Hz, 2H, CH¹(Cz)), 7.19 (ddd, *J* = 8.0, 7.1, 1.0 Hz, 2H, CH³(Cz)), 7.07 – 7.03 (m, 2H, *m*-ArH), 6.86 – 6.79 (m, 2H, *o*-ArH), 3.10 (sept, *J* = 6.7 Hz, 4H, CH(CH₃)₂), 1.91 (s, 6H, C(CH₃)₂), 1.47 (d, *J* = 6.8 Hz, 12H, CH(CH₃)₂), 1.22 (d, *J* = 6.8 Hz, 12H, CH(CH₃)₂). ¹³C NMR (101 MHz, acetone) δ 226.97 (NCN), 172.65 (C=O), 166.26 (ipso-Au-Ar), 145.63 (ipso-N-Ar(dipp)), 141.03 (ipso-N-Cz), 141.00 (*o*-Ar), 134.91 (*o*-Ar(dipp)), 133.99 (*m*-Ar), 130.24 (*p*-Ar(dipp)), 125.65 (*p*-Ar), 124.42 (*m*-Ar(dipp)), 124.18 (ipso-C-Cz), 122.90 (CH²(Cz)), 119.95 (CH⁴(Cz)), 119.35 (CH³(Cz)), 109.76 (CH¹(Cz)), 51.52 (C(CH₃)₂), 28.84 (CH(CH₃)₂), 24.42 (C(CH₃)₂), 23.66 (CH(CH₃)₂), 23.25 (CH(CH₃)₂). Elemental analysis calculated for C₄₈H₅₂AuN₃O₂: C, 64.06; H, 5.82; N, 4.67. found: C, 64.32; H, 6.04; N, 4.42.

(DAC)Au^(I)(4-diphenylaminophenyl) (**1c**): Method A, bright orange microcrystalline powder, yield 55 mg (85%). ¹H NMR (400 MHz, acetone) δ 7.53 (t, *J* = 7.8 Hz, 2H, *p*-ArH(dipp)), 7.40 (d, *J* = 7.7 Hz, 4H, *m*-ArH(dipp)), 7.21 – 7.11 (m, 4H, N(ArH)₂), 6.93 – 6.82 (m, 6H, N(ArH)₂), 6.62 – 6.55 (m, 2H, *m*-ArH), 6.53 – 6.45 (m, 2H, *o*-ArH), 3.05 (sept, *J* = 6.7 Hz, 4H, CH(CH₃)₂), 1.88 (s, 6H, C(CH₃)₂), 1.41 (d, *J* = 6.8 Hz, 12H, CH(CH₃)₂), 1.19 (d, *J* = 6.8 Hz, 12H, CH(CH₃)₂). ¹³C NMR (101 MHz, acetone) δ 227.28 (NCN), 172.65 (C=O), 161.91 (ipso-Au-Ar), 148.33 (*p*-Ar), 145.54 (ipso-N-Ar(dipp)), 144.37 (ipso-N-Ar), 140.73 (*o*-Ar), 134.89 (*o*-Ar(dipp)), 130.12 (*p*-Ar(dipp)), 128.88 (*p*-N(Ar)₂), 124.32 (*m*-Ar(dipp)), 123.25 (*m*-Ar), 123.01 (*o*-N(Ar)₂), 121.63 (*m*-N(Ar)₂), 51.39 (C(CH₃)₂), 28.80 (CH(CH₃)₂), 24.39 (C(CH₃)₂), 23.63 (CH(CH₃)₂), 23.20 (CH(CH₃)₂). Elemental analysis calculated for C₄₈H₅₄AuN₃O₂: C, 63.92; H, 6.03; N, 4.66. found: C, 63.52; H, 6.16; N, 4.66.

(MAC)Au^(I)(phenyl) (**2a**): Method A, white microcrystalline powder, yield 43 mg (81%). ¹H NMR (400 MHz, acetone) δ 7.50 – 7.38 (m, 2H, *p*-ArH(dipp)), 7.38 – 7.33 (m, 2H, *m*-ArH(dipp)), 7.32 – 7.26 (m, 2H, *m*-ArH(dipp)), 6.77 – 6.70 (m, 2H, *m*-ArH), 6.63 – 6.60 (m, 1H, *p*-ArH), 6.59 – 6.55 (m, 2H, *o*-ArH), 4.08 (s, 2H, CCH₂N), 3.41 (sept, *J* = 6.8 Hz, 2H, CH(CH₃)₂), 3.16 (sept, *J* = 6.8 Hz, 2H, CH(CH₃)₂),

1
2
3 1.60 (s, 6H, C(CH₃)₂), 1.44 (d, *J* = 6.8 Hz, 6H, CH(CH₃)₂), 1.41 (d, *J* = 6.9 Hz, 6H, CH(CH₃)₂), 1.36 (d, *J*
4 = 6.9 Hz, 6H, CH(CH₃)₂), 1.17 (d, *J* = 6.9 Hz, 6H, CH(CH₃)₂). ¹³C NMR (101 MHz, acetone) δ 221.42
5 (NCN), 172.23 (C=O), 167.65 (ipso-Au-Ar), 145.81 (ipso-N-Ar), 144.57 (ipso-N-Ar), 140.31 (*o*-Ar),
6 140.17 (*o*-Ar(dipp)), 136.06 (*o*-Ar(dipp)), 129.52 (*p*-Ar(dipp)), 129.11 (*p*-Ar(dipp)), 125.82 (*p*-Ar), 124.75
7 (*m*-Ar(dipp)), 123.69 (*m*-Ar(dipp)), 123.67 (*m*-Ar), 61.19 (CCH₂N), 37.91 (C(CH₃)₂), 28.69 (CH(CH₃)₂),
8 23.97 (CH(CH₃)₂), 23.92 (CH(CH₃)₂), 23.75 (C(CH₃)₂), 23.70 (CH(CH₃)₂), 23.13 (CH(CH₃)₂). Elemental
9 analysis calculated for C₃₆H₄₇AuN₂O: C, 59.99; H, 6.57; N, 3.89. found: C, 59.83; H, 6.69; N, 3.79.

10
11
12
13
14
15
16
17
18
19 (MAC)Au^(I)(4-carbazolyphenyl) (**2b**): Method A, white microcrystalline powder, yield 54 mg (83%).
20 ¹H NMR (400 MHz, acetone) δ 8.13 (dt, *J* = 7.8, 1.9 Hz 2H, CH⁴(Cz)), 7.54 – 7.43 (m, 2H, *p*-ArH(dipp)),
21 7.43 – 7.38 (m, 2H, CH²(Cz)), 7.37 – 7.29 (m, 4H, *m*-ArH(dipp)), 7.22 (dt, *J* = 8.3, 0.9 Hz, 2H, CH¹(Cz)),
22 7.18 (ddd, *J* = 8.0, 7.1, 1.0 Hz, 2H, CH³(Cz)), 7.03 – 6.97 (m, 2H, *m*-ArH), 6.92 – 6.85 (m, 2H, *o*-ArH), 4.13
23 (s, 2H, CCH₂N), 3.47 (sept, *J* = 6.8 Hz, 2H, CH(CH₃)₂), 3.22 (sept, *J* = 6.8 Hz, 2H, CH(CH₃)₂), 1.63 (s,
24 6H, C(CH₃)₂), 1.52 (d, *J* = 6.8 Hz, 6H, CH(CH₃)₂), 1.48 (d, *J* = 6.9 Hz, 6H, CH(CH₃)₂), 1.39 (d, *J* = 6.9 Hz,
25 6H, CH(CH₃)₂), 1.21 (d, *J* = 6.9 Hz, 6H, CH(CH₃)₂). ¹³C NMR (101 MHz, acetone) δ 220.69 (NCN),
26 172.25 (C=O), 167.91 (ipso-Au-Ar), 145.90 (ipso-N-Ar), 144.64 (ipso-N-Ar), 141.04 (ipso-N-Cz), 141.05
27 (*o*-Ar), 140.18 (*o*-Ar(dipp)), 136.09 (*o*-Ar(dipp)), 133.28 (*m*-Ar), 129.68 (*p*-Ar(dipp)), 129.27 (*p*-Ar(dipp)),
28 125.61 (*p*-Ar), 124.86 (*m*-Ar(dipp)), 124.08 (ipso-C-Cz), 123.82 (*m*-Ar(dipp)), 122.84 (CH²(Cz)), 119.92
29 (CH⁴(Cz)), 119.26 (CH³(Cz)), 109.79 (CH¹(Cz)), 61.24 (CCH₂N), 37.96 (C(CH₃)₂), 28.42 (CH(CH₃)₂),
30 24.10 (CH(CH₃)₂), 23.95 (C(CH₃)₂), 23.77 (CH(CH₃)₂), 23.74 (CH(CH₃)₂), 23.26 (CH(CH₃)₂). Elemental
31 analysis calculated for C₄₈H₅₄AuN₃O: C, 65.07; H, 6.14; N, 4.74. found: C, 64.67; H, 6.30; N, 4.68.

32
33
34
35
36
37
38
39
40
41
42
43
44
45
46
47 (MAC)Au^(I)(4-diphenylaminophenyl) (**2c**): Method A, beige microcrystalline powder, yield 55 mg (85%).
48 ¹H NMR (400 MHz, acetone) δ 7.49 – 7.38 (m, 2H, *p*-ArH(dipp)), 7.36 (d, *J* = 7.4 Hz, 2H, *m*-ArH(dipp)),
49 7.29 (d, *J* = 7.6 Hz, 2H, *m*-ArH(dipp)), 7.18 – 7.11 (m, 4H, N(ArH)₂), 6.90 – 6.82 (m, 6H, N(ArH)₂), 6.59
50 – 6.54 (br, 4H, ArH), 4.09 (s, 2H, CCH₂N), 3.42 (sept, *J* = 6.9 Hz, 2H, CH(CH₃)₂), 3.17 (sept, *J* = 7.0 Hz,
51 2H, CH(CH₃)₂), 1.61 (s, 6H, C(CH₃)₂), 1.46 (d, *J* = 6.8 Hz, 6H, CH(CH₃)₂), 1.42 (d, *J* = 6.9 Hz, 6H,
52
53
54
55
56
57
58
59
60

1
2
3 CH(CH₃)₂), 1.37 (d, *J* = 6.9 Hz, 6H, CH(CH₃)₂), 1.18 (d, *J* = 6.8 Hz, 6H, CH(CH₃)₂). ¹³C NMR (101 MHz,
4 acetone) δ 221.16 (NCN), 172.25 (C=O), 163.66 (ipso-Au-Ar), 148.41 (*p*-Ar), 145.82 (ipso-N-Ar), 144.58
5 (ipso-N-Ar(dipp)), 143.57 (ipso-N-Ar(dipp)), 140.77 (*o*-Ar), 140.18 (*o*-Ar(dipp)), 136.07 (*o*-Ar(dipp)),
6 (ipso-N-Ar(dipp)), 129.56 (*p*-Ar(dipp)), 129.15 (*p*-Ar(dipp)), 128.81 (*p*-N(Ar)₂), 124.79 (*m*-Ar(dipp)), 123.73 (*m*-Ar(dipp)),
7 123.61(*m*-Ar), 122.76 (*o*-N(Ar)₂), 121.36 (*m*-N(Ar)₂), 61.21 (CCH₂N), 37.91 (C(CH₃)₂), 28.70 (CH(CH₃)₂),
8 28.37 (CH(CH₃)₂), 24.05 (CH(CH₃)₂), 23.91 (C(CH₃)₂), 23.75 (CH(CH₃)₂), 23.70 (CH(CH₃)₂), 23.21
9 (CH(CH₃)₂). Elemental analysis calculated for C₄₈H₅₆AuN₃O: C, 64.93; H, 6.36; N, 4.73. found: C, 64.91;
10 H, 6.40; N, 4.84.
11
12
13
14
15
16
17
18
19

20
21 (MAC)Au^(I)(4-dimethylaminophenyl) (**2d**): Method A, beige microcrystalline powder, yield 45 mg (80%).
22
23 ¹H NMR (400 MHz, acetone) δ 7.49 – 7.38 (m, 2H, *p*-ArH(dipp)), 7.35 (d, *J* = 7.6 Hz, 2H, *m*-ArH(dipp)),
24 7.28 (d, *J* = 7.6 Hz, 2H, *m*-ArH(dipp)), 6.47 – 6.41 (m, 2H, *m*-ArH), 6.32 – 6.26 (m, 2H, *o*-ArH), 4.04 (s,
25 2H, CCH₂N), 3.40 (sept, *J* = 6.9 Hz, 2H, CH(CH₃)₂), 3.16 (sept, *J* = 6.9 Hz, 2H, CH(CH₃)₂), 2.66 (s, 6H,
26 N(CH₃)₂), 1.60 (s, 6H, C(CH₃)₂), 1.44 (d, *J* = 6.8 Hz, 6H, CH(CH₃)₂), 1.40 (d, *J* = 6.9 Hz, 6H, CH(CH₃)₂),
27 1.36 (d, *J* = 6.9 Hz, 6H, CH(CH₃)₂), 1.17 (d, *J* = 6.9 Hz, 6H, CH(CH₃)₂). ¹³C NMR (101 MHz, acetone) δ
28 222.06 (NCN), 172.29 (C=O), 155.16 (ipso-Au-Ar), 148.31 (*p*-Ar), 145.79 (ipso-N-Ar(dipp)), 144.58
29 (ipso-N-Ar(dipp)), 140.42 (*o*-Ar), 140.26 (*o*-Ar(dipp)), 136.12 (*o*-Ar(dipp)), 129.42 (*p*-Ar(dipp)), 129.01
30 (*p*-Ar(dipp)), 124.70 (*m*-Ar(dipp)), 123.63 (*m*-Ar(dipp)), 112.20 (*m*-Ar), 61.16 (CCH₂N), 40.28 (N(CH₃)₂),
31 37.90 (C(CH₃)₂), 28.68 (CH(CH₃)₂), 23.97 (CH(CH₃)₂), 23.92 (C(CH₃)₂), 23.75 (CH(CH₃)₂), 23.70
32 (CH(CH₃)₂), 23.13 (CH(CH₃)₂). Elemental analysis calculated for C₃₈H₅₂AuN₃O: C, 59.75; H, 6.86; N, 5.50.
33 found: C, 59.47; H, 6.92; N, 5.53.
34
35
36
37
38
39
40
41
42
43
44
45

46
47 (MAC)Au^(I)(julolidine) (**2e**): Method A, yellow microcrystalline powder, yield 51 mg (55%). ¹H NMR (400
48 MHz, acetone) δ 7.47 – 7.37 (m, 2H, *p*-ArH(dipp)), 7.35 – 7.31 (m, 2H, *m*-ArH(dipp)), 7.27 (d, *J* = 7.7 Hz,
49 2H, *m*-ArH(dipp)), 5.97 (s, 2H, *o*-ArH), 4.01 (s, 2H, CCH₂N), 3.39 (sept, *J* = 6.9 Hz, 2H, CH(CH₃)₂), 3.15
50 (sept, *J* = 6.9 Hz, 2H, CH(CH₃)₂), 2.89 – 2.83 (m, 4H, ArCH₂CH₂), 2.34 (t, *J* = 6.6 Hz, 4H, NCH₂CH₂),
51 1.79 – 1.71 (m, 4H, CH₂CH₂CH₂), 1.58 (s, 6H, C(CH₃)₂), 1.44 (d, *J* = 6.8 Hz, 6H, CH(CH₃)₂), 1.40 (d, *J* =
52
53
54
55
56
57
58
59
60

6.9 Hz, 6H, CH(CH₃)₂), 1.35 (d, *J* = 6.9 Hz, 6H, CH(CH₃)₂), 1.17 (d, *J* = 6.9 Hz, 6H, CH(CH₃)₂). ¹³C NMR (101 MHz, acetone) δ 222.36 (NCN), 172.29 (C=O), 154.39 (ipso-Au-Ar), 145.73 (ipso-N-Ar(dipp)), 144.52 (ipso-N-Ar(dipp)), 140.29 (*p*-Ar), 140.24 (*o*-Ar(dipp)), 138.93 (*o*-Ar), 136.13 (*o*-Ar(dipp)), 129.36 (*p*-Ar(dipp)), 128.94 (*p*-Ar(dipp)), 124.68 (*m*-Ar(dipp)), 123.61 (*m*-Ar(dipp)), 119.07 (*m*-Ar), 61.22 (CCH₂N), 50.18 (NCH₂CH₂), 37.86 (C(CH₃)₂), 28.67(CH(CH₃)₂), 27.46 (CH₂CH₂CH₂), 24.02 (CH(CH₃)₂), 23.90 (C(CH₃)₂), 23.76 (CH(CH₃)₂), 23.68 (CH(CH₃)₂), 23.16 (CH(CH₃)₂), 22.72 (CH₂CH₂CH₂). Elemental analysis calculated for C₄₂H₅₆AuN₃O: C, 61.83; H, 6.92; N, 5.15. found: C, 61.48; H, 6.89; N, 5.15.

(MAC)Au^(I)(4-dimethylamino-2,5-dimethylphenyl) (**2d-Me**): Method A, light yellow microcrystalline powder, yield 38 mg (65%). ¹H NMR (400 MHz, acetone) δ 7.47 – 7.38 (m, 2H, *p*-ArH(dipp)), 7.38 – 7.34 (m, 2H, *m*-ArH(dipp)) 7.31 – 7.27 (m, 2H, *m*-ArH(dipp)), 6.08 (s, 2H, *m*-ArH), 4.02 (s, 2H, CCH₂N), 3.42 (sept, *J* = 6.8 Hz, 2H, CH(CH₃)₂), 3.17 (sept, *J* = 6.8, 2H, CH(CH₃)₂), 2.64 (s, 6H, N(CH₃)₂), 1.59 (s, 6H, C(CH₃)₂), 1.42 (d, *J* = 6.8 Hz, 6H, CH(CH₃)₂), 1.39 – 1.33 (m, 18H, CH(CH₃)₂ and *o*-ArCH₃), 1.17 (d, *J* = 6.9 Hz, 6H, CH(CH₃)₂). ¹³C NMR (101 MHz, acetone) δ 223.71 (NCN), 172.47 (C=O), 156.91 (ipso-Au-Ar), 148.80 (*p*-Ar), 147.28 (*o*-Ar), 145.78 (ipso-N-Ar(dipp)), 144.62 (ipso-N-Ar(dipp)), 140.83 (*o*-Ar(dipp)), 136.53 (*o*-Ar(dipp)), 129.44 (*p*-Ar(dipp)), 129.13 (*p*-Ar(dipp)), 124.85 (*m*-Ar(dipp)), 123.81 (*m*-Ar(dipp)), 110.17 (*m*-Ar), 61.54 (CCH₂N), 40.28 (N(CH₃)₂), 37.77 (C(CH₃)₂), 28.63 (CH(CH₃)₂), 28.40 (CH(CH₃)₂), 25.73 (ArCH₃), 23.89 (CH(CH₃)₂), 23.85 (C(CH₃)₂), 23.80 (CH(CH₃)₂), 23.54 (CH(CH₃)₂), 23.17 (CH(CH₃)₂). Elemental analysis calculated for C₄₀H₅₆AuN₃O: C, 60.67; H, 7.13; N, 5.31. found: C, 60.67; H, 7.43; N, 5.17.

(MAC)Au^(I)(2,5-dimethyljulolidine) (**2e-Me**): Method B, yellow microcrystalline powder, yield 35 mg (56%). ¹H NMR (400 MHz, acetone) δ 7.47 – 7.37 (m, 2H, *p*-ArH(dipp)), 7.36 – 7.33 (m, 2H, *m*-ArH(dipp)), 7.30 – 7.26 (m, 2H, *m*-ArH(dipp)), 4.00 (s, 2H, CCH₂N), 3.42 (sept, *J* = 6.8 Hz, 2H, CH(CH₃)₂), 3.17 (sept, *J* = 6.8 Hz, 2H, CH(CH₃)₂), 2.80 – 2.74 (m, 4H, ArCH₂CH₂), 2.24 (t, *J* = 6.8 Hz, 4H, NCH₂CH₂), 1.79 (m, 4H, CH₂CH₂CH₂), 1.59 (s, 6H, C(CH₃)₂), 1.41 (d, *J* = 6.8 Hz, 6H, CH(CH₃)₂), 1.36 (d, *J* = 6.9 Hz, 12H, CH(CH₃)₂), 1.24 (s, 6H, *o*-ArCH₃), 1.18 (d, *J* = 6.9 Hz, 6H, CH(CH₃)₂). ¹³C NMR

(101 MHz, acetone) δ 223.76 (NCN), 172.50 (C=O), 158.73 (ipso-Au-Ar), 145.75 (ipso-N-Ar(dipp)), 144.58 (ipso-N-Ar(dipp)), 142.49 (*p*-Ar), 141.38 (*o*-Ar), 140.96 (*o*-Ar(dipp)), 136.63 (*o*-Ar(dipp)), 129.44 (*p*-Ar(dipp)), 129.13 (*p*-Ar(dipp)), 124.90 (*m*-Ar(dipp)), 123.86 (*m*-Ar(dipp)), 116.23 (*m*-Ar), 61.51 (CCH₂N), 50.25 (NCH₂CH₂), 37.77 (C(CH₃)₂), 29.67 (CH₂CH₂CH₂), 28.62 (CH(CH₃)₂), 28.40 (CH(CH₃)₂), 26.01 (ArCH₃), 23.89 (CH(CH₃)₂), 23.79 (C(CH₃)₂), 23.56 (CH(CH₃)₂), 23.21 (CH(CH₃)₂), 23.15 (CH(CH₃)₂), 22.99 (CH₂CH₂CH₂). Elemental analysis calculated for C₄₄H₆₀AuN₃O: C, 62.62; H, 7.17; N, 4.98. found: C, 62.64; H, 7.47; N, 4.83.

X-ray Crystallography. The X-ray intensity data were collected on a Bruker APEX DUO 3-circle platform diffractometer with the χ -axis fixed at 50.74°, and using Mo K_{α} radiation ($\lambda = 0.71073$ Å) from a fine-focus tube monochromatized by a TRIUMPH curved-crystal monochromator. The diffractometer was equipped with an APEX II CCD detector and an Oxford Cryosystems Cryostream 700 apparatus for low-temperature data collection adjusted to 100(2) K. The crystal was mounted in a Cryo-Loop using Paratone oil. A complete hemisphere of data was scanned on omega (0.5°) at a detector distance of 50 mm and a resolution of 512 x 512 pixels. The frames were integrated using the SAINT algorithm to give the hkl files corrected for Lp/decay. Data were corrected for absorption effects using the multi-scan method (SADABS). The structures were solved by intrinsic phasing and refined with the Bruker SHELXTL Software Package. Supplementary crystallographic data can be downloaded from Cambridge Crystallographic Data Centre (CCDC) with the registration number: 1948368 (**2a**), 1948367 (**2b**), 1948366 (**1a**), 1948365 (**1b**), 1948370 (**1c**), 1948369 (**2d**), 1948371 (**2d-Me**) and 1948372 (**2e-Me**).

Theoretical Calculations. All Density Functional Theory (DFT) calculations reported in this work were performed using the Q-Chem 5.1 program.¹⁹ Ground state geometry optimization of the complexes were performed at the B3LYP/LACVP* level. Time-dependent density functional theory (TD-DFT) calculations were performed on the ground state optimized geometries at the CAM-B3LYP/LACVP* level which has been found to offer good agreement with experimental results for the class of materials under study striking a balanced description of both charge-transfer and locally excited (LE) states.^{1a-c} Relaxed potential energy

1
2
3 surface (PES) scans were performed at the B3LYP/LACVP** level. The PES scans were performed for the
4 complexes in 15° increments of the dihedral angle between the C-N bond of the carbene and the C-C bond
5 of the Aryl ligand that includes the coordinating C atom and the adjacent C atom. Single-point calculations
6 were performed on the geometries optimized for each dihedral angle constraint using the B3LYP functional
7 with Grimme's D3 dispersion correction²⁰ and the LACVP** ECP/basis set to account for dispersion effects
8 which are vital to reliably predict the potential energy landscape.
9
10
11
12
13
14
15

16 **Electrochemical Measurements.** Cyclic voltammetry (CV) and differential pulsed voltammetry (DPV)
17 were conducted using a VersaSTAT 3 Potentiostat Galvanostat with a standard three-electrode system. A
18 glassy carbon rod was used as the working electrode, a platinum wire as the counter electrode and a silver
19 wire as a pseudo-reference electrode. Anhydrous acetonitrile (CH₃CN, DriSolv from VWR) was used as
20 solvent and 0.1 M tetra-*n*-butyl ammonium hexafluorophosphate (TBAF from Acros) was used as the
21 supporting electrolyte. Decamethylferrocene was used as internal reference. The redox potentials were
22 obtained based on values measured from DPV and are reported relative to a ferrocene/ferrocenium (Fc⁺/Fc)
23 redox couple.
24
25
26
27
28
29
30
31
32
33

34 **Photophysical Characterization.** UV-visible absorption spectra were recorded using a Hewlett-Packard
35 8453 diode array spectrometer. Steady-state photoluminescent emission spectra were measured on a Photon
36 Technology International QuantaMaster model C-60 fluorimeter. Transient photoluminescent lifetimes
37 were measured on an IBH Fluorocube instrument using time-correlated single-photon counting method
38 (TCSPC) for measurements at ambient conditions and multichannel scaling method (MSC) for
39 measurements at low temperature. Photoluminescent quantum yields were determined using a Hamamatsu
40 C9920 system equipped with a xenon lamp, calibrated integrating sphere and model C10027 photonic
41 multichannel analyzer (PMA). Temperature-dependent lifetime measurements from 77 to 310 K were
42 measured using IBH Fluorocube instrument in an OptistatDN Oxford cryostat. All fluid samples for
43 photoluminescent measurements were deaerated by bubbling N₂ in a glass cuvette fitted with a Teflon
44 stopcock. Doped polymer films (1 wt%) were prepared in toluene solution of polystyrene (PS). Solutions
45
46
47
48
49
50
51
52
53
54
55
56
57
58
59
60

were dropcast onto a quartz substrate and the films were air-dried for 3 h before drying under vacuum overnight. The polymer films were measured under a stream of N₂ during the photophysical measurements.

Results and Discussion

Synthesis and Characterization

A series of two-coordinate (carbene)Au(aryl) complexes with DAC (**1a–c**) and MAC (**2a–e**, **2d-Me** and **2e-Me**) as an electron acceptor ligands were synthesized as shown in Figure 2. The aryl moieties are phenyl (**1a** and **2a**), 4-carbazolyl phenyl (**1b** and **2b**), 4-diphenylamino-phenyl (**1c** and **2c**), 4-dimethylamino-phenyl (**2d**), julolidine (**2e**), 2,6-dimethyl-4-dimethylamino-phenyl (**2d-Me**) and 3,5-dimethyl-julolidine (**2e-Me**). All of the complexes were isolated in good yields (56–85%) via a modified one-pot reaction by reaction of the (carbene)AuCl precursor with aryl boronic acid or pinacol ester in the presence of KOH, as shown in Figure 2.²¹ The conversion of the Au precursor complex was monitored by ¹H NMR and the final desired products were purified by recrystallization. When boronic acid is a reactant, 100% conversion of the precursor can be realized within 3 h. However, the reaction time needs to be extended to 12 h if pinacol-borane is used instead, due to the relatively lower reactivity of the boronic acid ester. Less boronic acid ester (1.2 equiv) is required than boronic acid (1.5 equiv.) for 100% conversion of

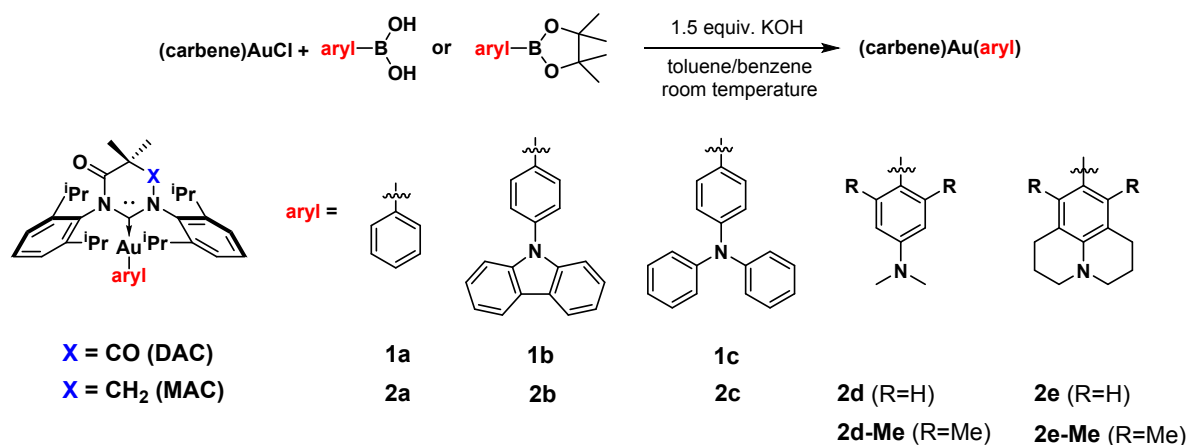


Figure 2. Preparation of two-coordinate (carbene)Au(aryl) complexes and the molecular structures of complexes **1a–c**, **2a–e**, **2d-Me** and **2e-Me**.

the (carbene)AuCl precursor. The complexes were isolated as beige to orange solids and are stable to air in solution and solid state.

Selected metrical parameters from single crystal structures of **1a–c**, **2a–b** and **2d** are given in Figure 3. All of the molecules have a linear coordination geometry at the Au center ($C_{\text{carbene}}-\text{Au}-C_{\text{aryl}} = 175-178^\circ$). Bond lengths between Au and C_{carbene} (2.01–2.06 Å) are similar to values between Au and C_{aryl} (2.02–2.05 Å). The dihedral angle between the carbene ligand and the coordinated phenylene is smaller in **1a** (17.6°), **2a** (13.3°), **1b** (2.7°) and **2b** (4.1°) than in **1c** (52.0°) and **2d** (62.5°). Space-filling models of **1a–c** in Figure 3 illustrate that the coordinated phenyl moieties are not sterically encumbered by the bulky dipp (diisopropyl phenyl) moieties, and thus a small energy barrier is expected for the rotation around the Au– C_{aryl} bond in these derivatives. Steric interactions among aryl groups lead to larger dihedral angles between the coordinated aryl and the amines in **1b**, **2b** and **1c** (48.8°, 52.6° and 34.2°, respectively) than the dimethylamine in **2d** (10.3°).

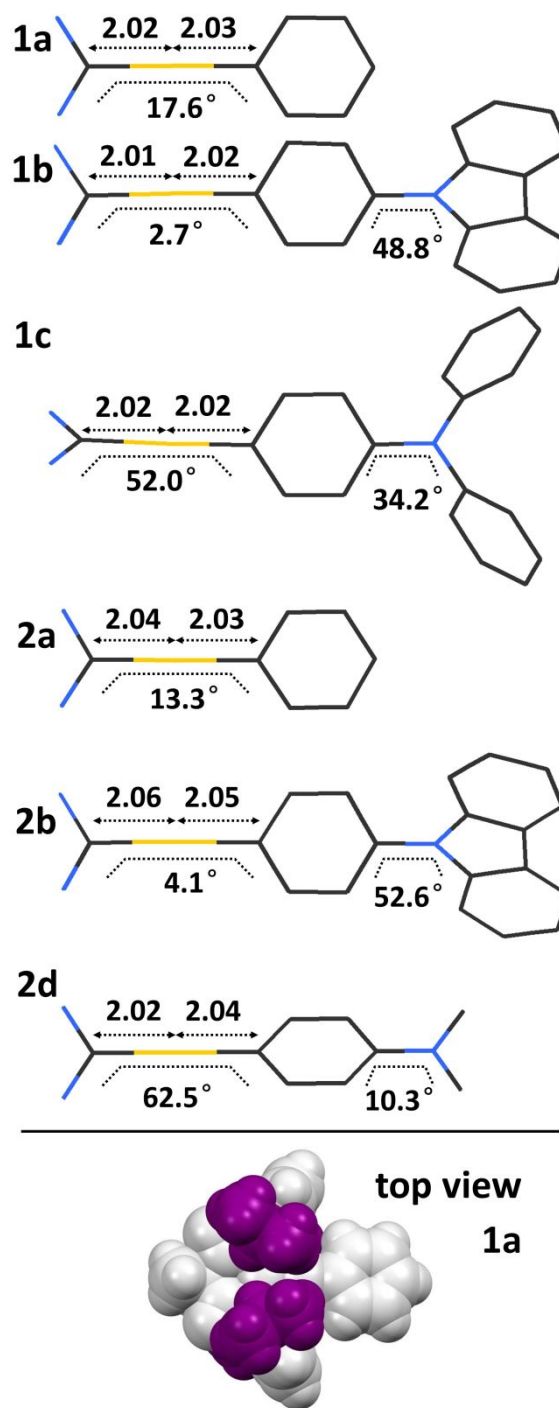


Figure 3. (top) Simplified geometries of **1a–c**, **2a**, **2b** and **2d** with significant crystallographic distances (in Å) and angles, C: grey; N: blue, Au: gold; (bottom) space-filling diagrams of **1a**, the isopropyl moieties are highlighted in purple.

1
2
3 Electrochemical properties of complexes **1a–c** and **2a–d** were investigated by cyclic voltammetry and
4 differential pulse voltammetry (DPV) in acetonitrile. Redox potentials determined using
5 decamethylferrocene as internal reference are reported here along with those for the (DAC)AuCl and
6 (MAC)AuCl precursors relative to ferrocene (Table 1). The complexes display irreversible oxidation and
7 quasi-reversible reduction peaks (see ESI). The oxidation potentials of **1a**, **1b** and **1c** decrease from 0.93 to
8 0.72 to 0.28 V, respectively, and are similar to values found for the corresponding MAC derivatives (**2a–**
9 **c**). The complexes with phenyl ligands (**1a** and **2a**) have oxidation potentials within 0.04 V of the
10 (carbene)AuCl analogs, indicating that the oxidation is metal centered. The small cathodic shift in oxidation
11 potential of the phenyl-carbazole derivatives (**1b** and **2b**, $\Delta E_{\text{ox}} = 0.2$ V) suggests that the HOMO in these
12 complexes is comprised of contributions from both the metal and aryl ligand. The oxidation potentials for
13 the remaining complexes (**1c**, **2c** and **2d**) are shifted cathodically from the (carbene)AuCl analogs by
14 0.6–0.9 V, indicating that the HOMO in these complexes is primarily based on the arylamine ligand and
15 have little metal character. The reduction potentials for **1a–c** fall between -1.53 V and -1.71 V, close to that
16 of (DAC)AuCl, and similarly, potentials for **2a** and **2c** are close to that of (MAC)AuCl ($E_{\text{red}} = -2.42$ V).
17 The redox properties indicate that the oxidation is gradually tuned from metal centered to aryl-amine ligand
18 based, depending on the amine, whereas the reduction potential is dictated mainly by the carbene ligand.
19
20
21
22
23
24
25
26
27
28
29
30
31
32
33
34
35
36
37
38
39
40
41
42
43
44
45
46
47
48
49
50
51
52
53
54
55
56
57
58
59
60

Table 1. Electrochemical data of (carbene)AuCl precursors and (carbene)Au(aryl) complexes.^a

Complex	E_{ox} (V) ^a	E_{red} (V) ^a	$E_{\text{ox}}-E_{\text{red}}$ (V)
(DAC)AuCl	0.97	-1.56	2.53
1a	0.93	-1.53	2.46
1b	0.72	-1.71	2.43
1c	0.28	-1.55	1.83
(MAC)AuCl	0.95	-2.44	3.39
2a	0.92	-2.42	3.34
2b	0.73	b	b
2c	0.26	-2.41	2.67
2d	-0.03	-2.45	2.42
2d-Me	-0.10	b	b
2e	-0.20	b	b
2e-Me	-0.28	b	b

^a Values obtained from DPV measurements carried out using decamethylferrocene as an internal reference, with redox potentials adjusted to 0 V versus ferrocene.²² The redox potential measured for decamethylferrocene relative to ferrocene can be found in the ESI. ^b No reduction peak is observed.

Turning the Renner–Teller Effect On and Off

The Renner–Teller effect will bring about a bending distortion in a linear two coordinate complex that have a lowest excited state with MLCT character (Au d_{z^2} -to-ligand) such as a (carbene)Au(aryl) complex. In order to probe this distortion in a basic system we considered a representative analog of the compounds investigated here, containing a simplified MAC ligand with the dipp moieties replaced by methyl groups. Two triplet optimized structures were identified using unrestricted DFT (UDFT) calculations at the B3LYP/LACVP* level, one remains linear with elongated Au–C bonds, whereas the other is bent ($C_{\text{carbene}}-\text{Au}-C_{\text{aryl}} = 145^\circ$). Here we find major differences between the SOMO and SOMO-1 orbitals of the two structures (SOMO = highest occupied singly occupied molecular orbital) as shown in Figure 4(a). The geometric change from linear to bent is the result of σ - π mixing in the excited state. The SOMO of the linear triplet is largely localized on a π -orbital that has carbene-Au antibonding character, whereas the SOMO-1 is a combination of Au d_{z^2} and Au–ligand σ -orbitals. Bending the $C_{\text{carbene}}-\text{Au}-C_{\text{aryl}}$ angle stabilizes the SOMO sufficiently to overcome a smaller destabilization of the SOMO-1 in the T_1 state and leads to a structure that is 0.35 eV lower in total energy than the linear one. The excited state of the bent molecule can then undergo effective nonradiative deactivation via vibronic coupling with the ground state. In

contrast, no equivalent stabilization in the excited state is generated by bending in complexes that have an ICT excited state. The carbene and arene π orbitals involved in the ICT transition are spatially well-separated and there is only a minor contribution of metal d_{xz} orbitals in the HOMO. Such an excited molecule with ICT character can thus decay radiatively back to the ground state with a high efficiency as deactivation by a vibronic coupling pathway is suppressed.

To probe the Renner–Teller effect in these complexes, we consider **1a–c** and **2a–d**. According to the electrochemical measurements in this series of complexes, electron donating substituents on the aryl ring can be used to alter the composition of the HOMO from one that is Au d orbital in nature to one dominated by the aryl π system. Thus, the position of the lowest excited state can be inverted from MLCT to ICT state. It is noteworthy that the higher lying intraligand π - π^* states never become the lowest excited state in these complexes. Time-dependent density functional theory (TD-DFT) calculations were carried out using the optimized ground state geometries to clarify the nature of the singlet and triplet excited states (Table 2). Representative natural transition orbitals (NTOs) for the S_1 state of **1a** and **1c** are shown in Figure 4(b). These isosurfaces represent the electronic structure of the molecules immediately after

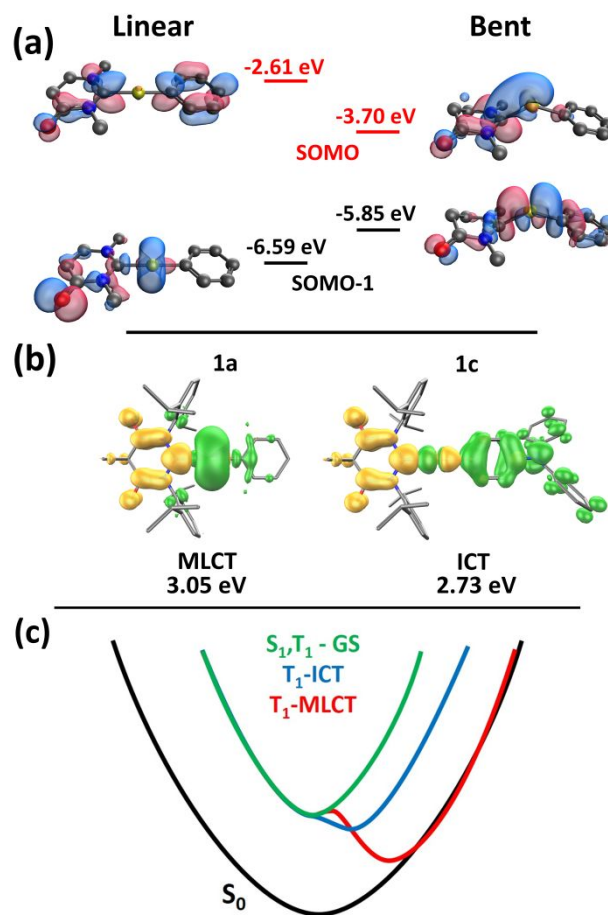


Figure 4. (a) Schematic diagram of the frontier molecular orbitals of a simplified MAC:→Au(C₆H₅) model complex illustrating the Renner–Teller effect. (b) NTOs for the lowest singlet excited states of **1a** and **1c** (green: hole, yellow: electron), with both molecules in the ground state geometry (note that **1a** will ultimately distort to the bent structure in the excited state) (c) Qualitative energy level diagram for ICT and MLCT based T_1 potential energy surfaces (GS = ground state geometry), based on TD-DFT calculations.

excitation, before either ISC or a Renner-Teller distortion can take place. The NTOs of **1a** show substantial MLCT character whereas those of **1c** are characteristic of an ICT state. In addition to investigating the S_1 and T_1 states in the optimized ground state geometry, we have optimized the geometry of the triplet state for each molecule (Table 2). The T_1 states predicted for complexes **2b** and **2c** in the ground state geometry are localized on the aryl ligands, but become MLCT and ICT based T_1 states, respectively, in the optimized triplet geometry. The optimized T_1 geometries in **1a-b** and **2a-b** present a significant bending distortion at the Au center (the $C_{\text{carbene}}\text{-Au-C}_{\text{aryl}}$ angle is as small as 137° in **2a**), which is attributed to the Renner-Teller effect. In contrast, this angle close to 180° in the complexes that have ICT based T_1 states, *i.e.* **1c**, **2c**, **2d-2e**. Stabilization of the geometry optimized triplet is much greater for the (carbene)Au(aryl) complexes with MLCT T_1 states (1.6-2.1 eV) than for the ICT based triplet states (0.5-0.8 eV). The increased stabilization of the bent structure for the MLCT triplets leads to enhanced vibronic coupling between the excited and ground states, resulting in the markedly higher nonradiative decay rates observed for MLCT based triplet states. A qualitative energy level diagram with the ground state geometry S_1/T_1 , as well as ICT and MLCT

Table 2. The lowest singlet and triplet excited state properties determined from TD-DFT calculations.

Complex	Based on optimized S_0 geometry				Based on optimized T_1 geometry			
	S_1		T_1		T_1			
	Energy (eV / f)	State	Energy (eV)	State	C-Au-X ($^\circ$) ^a	Energy (eV)	State	ΔE (eV) ^d
(DAC)AuCl	3.46 / 0.003	MLCT	3.14	MLCT	168	2.62	MLCT	0.52
1a	3.15 / 0.003	MLCT	3.04	MLCT	138	1.11	MLCT	1.93
1b	3.28 / 0.004	MLCT	3.06	MLCT	141	1.36	MLCT	1.70
1c	2.93 / 0.248	ICT	2.66	ICT	179	2.12	ICT	0.54
(MAC)AuCl	4.12 / 0.005	MLCT	3.43	MLCT	162	2.80	MLCT	0.63
2a	3.92 / 0.006	MLCT	3.40	MLCT	137	1.33	MLCT	2.07
2b	4.00 / 0.007	MLCT	3.06	LC(Cz) ^b	140	1.43	MLCT	1.63
2c	3.72 / 0.346	ICT	3.06	LC(TPA) ^c	179	2.55	ICT	0.51
2d	3.47 / 0.316	ICT	3.03	ICT	167	2.26	ICT	0.77
2d-Me	3.36 / 0.299	ICT	2.96	ICT	177	2.19	ICT	0.77
2e	3.36 / 0.306	ICT	2.89	ICT	179	2.34	ICT	0.55
2e-Me	3.25 / 0.283	ICT	2.83	ICT	179	2.12	ICT	0.71

^a The bond angle is for $C_{\text{carbene}}\text{-Au-Cl}$ or $C_{\text{carbene}}\text{-Au-C}_{\text{aryl}}$. ^b Cz = carbazolyl. ^c This state is predominantly localized on the triphenyl amine (TPA) with a small amount of ICT character. ^d The difference in vertical transition energy between triplet states in the optimized S_0 and T_1 structures.

1
2
3 T_1 surfaces, is shown Figure 4(c). The figure illustrates how bending in the MLCT state brought about by
4 the Renner-Teller effect promotes the nonradiative $T_1 \rightarrow S_0$ transition.
5
6
7

8 Absorption spectra of **1a–c** and **2a–d** in THF solution are given in Figure 5a. The intense absorption
9 bands in high energy region (below 280 nm) correspond to the ligand-based $\pi\text{-}\pi^*$ transitions for all the
10 chromophores. The broad featureless band ($\epsilon \sim 3000 \text{ L}/(\text{mol}\times\text{cm})$) peaking at 350 nm in **1a** and 290 nm in
11 **2a** is assigned to ^1ICT absorption from the phenyl to the carbene ligand. Weak bands ($\epsilon \sim 500 \text{ L}/(\text{mol}\times\text{cm})$)
12 at lower energy (390–440 nm in **1a** and 330–360 nm in **2a**) are assigned to the $^1\text{MLCT}$ absorption, which
13 agree well with the $^1\text{MLCT}$ bands of the corresponding (carbene)AuCl precursors (see Figure S9 in the
14 ESI). Structured bands between 295–350 nm in **1b** and **2b** are assigned to the $\pi\text{-}\pi^*$ transitions localized on
15 the carbazolyl moiety. The lowest-lying $^1\text{MLCT}$ bands are overlapped by the close-lying and more intense
16 ^1ICT band peaking at 390 nm in **1b** and 330 nm in **2b**. For **1c** and **2c**, intense bands at 300 nm are assigned
17 to $\pi\text{-}\pi^*$ transitions on the TPA moiety and the lowest lying ^1ICT bands peak at 460 nm in **1c** and at 360 nm
18 in **2c**. The ICT band of **2d** is slightly redshifted in comparison to that of **2c**, peaking at 365 nm. This shift
19 is attributed to the stronger electron-donating strength of the dimethyl amino group and the resultant
20 destabilized HOMO energy level. The distinct ^1ICT bands in these complexes present characteristic
21 bathochromic shifts in solvents with decreasing polarity (from CH_3CN to THF to cyclohexane) as shown
22 in Figure 5b. In contrast, the ligand-based absorption bands at 340 nm in **1b** and 300 nm in **1c** do not shift
23 in these solvents. The pronounced negative solvatochromism of the ^1ICT bands is rationalized to the effects
24 of opposing molecular dipole moments in the ground and excited states, which result in an increase in
25 excitation energy in polar solvents.^{1a, 1c}
26
27
28
29
30
31
32
33
34
35
36
37
38
39
40
41
42
43
44
45

46 Luminescence at room temperature from **1a–b** and **2a–b** is broad and featureless (see ESI). The
47 emission is weak ($\Phi_{\text{PL}} < 0.001$) with short luminescence decay lifetimes ($\tau < 10 \text{ ns}$) in both fluid solution
48 and polystyrene (PS) film. Emission from **2b** at room temperature ($\lambda_{\text{max}} = 389 \text{ nm}$ in PS) is significantly
49 higher in energy than that from **1a–b** and **2a** ($\lambda_{\text{max}} > 450 \text{ nm}$ in PS). The emission energy in PS at 77 K
50 remains relatively constant for **1a–b** and **2a** and the luminescence lifetimes are several tens of microseconds,
51
52
53
54
55
56
57
58
59
60

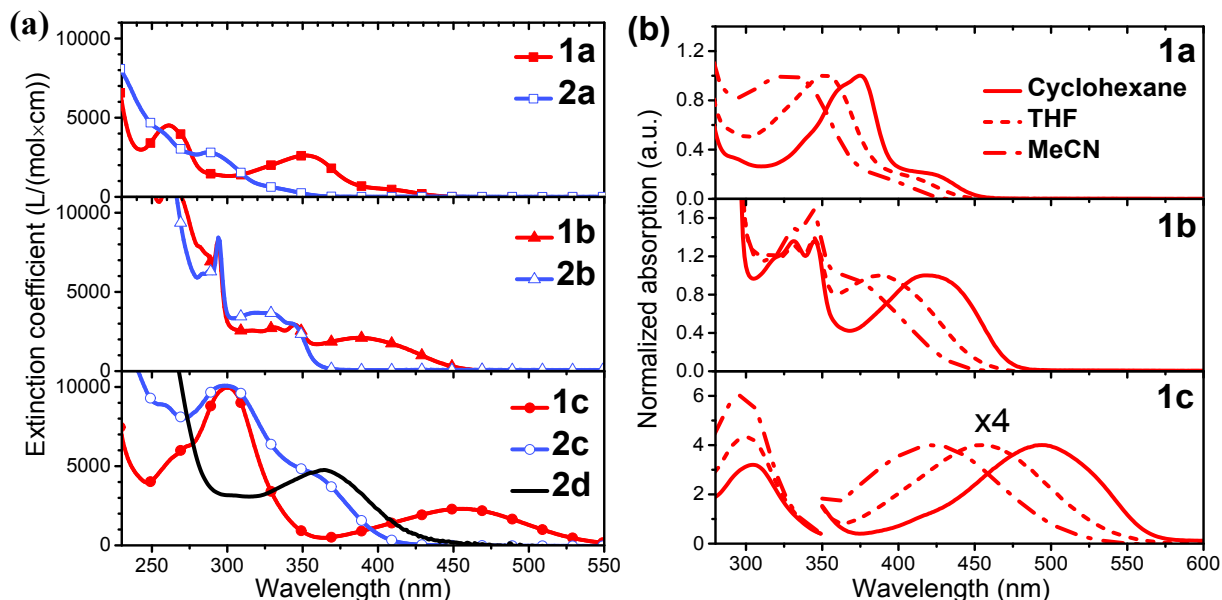


Figure 5. (a) UV-visible absorption spectra of complexes **1a–c** and **2a–d** in THF at RT; (b) bathochromic shift of the ICT absorption bands with decreasing solvent polarity in complexes **1a–c**.

indicative of phosphorescence. In contrast, emission from **2b** at 77 K is red shifted ($\lambda_{\text{max}} = 410$ nm) and highly structured, with a decay lifetime of seconds. The luminescence data for **1a–b** and **2a** in PS are consistent with assignment to MLCT transitions, whereas emission from **2b** is ascribed to a transition localized on the PhCz ligand. We propose that the poor luminescence efficiency of **1a–b** and **2a** is a result of rapid nonradiative decay caused by a bending distortion of the $\text{C}_{\text{carbene}}\text{–Au–C}_{\text{aryl}}$ bond in the excited state (Renner-Teller effect). This deactivation pathway is so effective that the process is not suppressed by the relatively rigid polymer matrix. It is inferred that the large MAC/DAC ligands provide sufficient steric bulk to allow the bending distortion of the smaller aryl ligands within the free volume of the polymer matrix, resulting in rapid decay of the excited state ($k_{\text{nr}} \sim 10^8 \text{ s}^{-1}$) in both polymer film and fluid solution.

In contrast, complexes **1c**, **2c** and **2d** present bright orange, blue and green emission, respectively, featuring broad unstructured bands in both fluid solution and PS film at room temperature. Emission spectra in 2-methyltetrahydrofuran (MeTHF) and methylcyclohexane (MeCy) are shown in Figure 6 and the corresponding photophysical properties are summarized in Table 2. At room temperature, the broad ICT emission bands undergo hypsochromic shifts with decreasing solvent polarity, as well as in frozen solvents

at 77 K. The solvatochromism and rigidochromism is caused by the dipolar solvent organizing around the large dipole of the S_0 ground state, destabilizing the opposing dipole of the emissive ICT state (see ESI). Thus, hypsochromic shifts at 77 K are greater in a polar solvent than a non-polar solvent. Complex **2c** displays a structured emission band at 77 K, presumably owing to mixing between the ICT state and ligand-centered (3LC) state of the TPA moiety, whereas spectra from **1c** and **2d** at 77 K remain featureless. All three complexes present broad emission spectra at both room temperature and low temperature when doped into a PS film

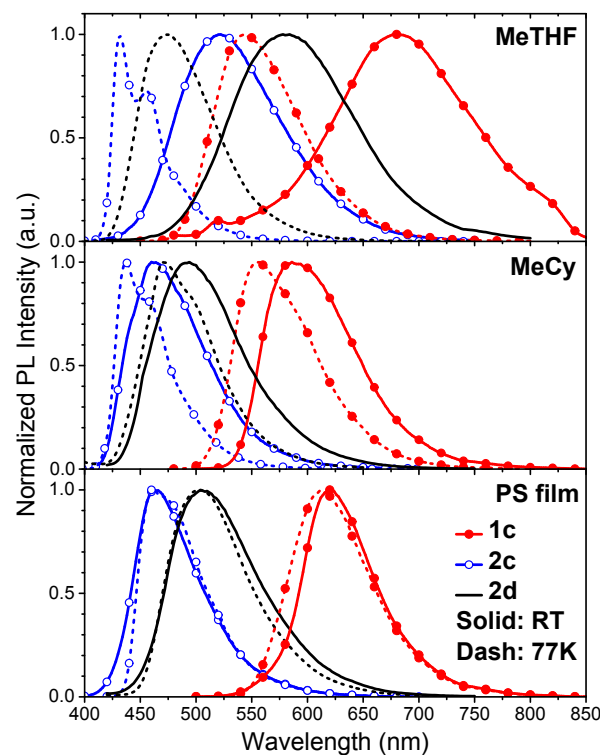


Figure 6. Emission spectra of complex **1c**, **2c** and **2d** at room temperature and 77 K in dilute fluid solution and polystyrene (PS) film.

(Figure 6). Large increases in luminescence lifetimes (from μs to tens of μs) upon cooling to 77 K are indicative of emission from a thermally populated ^1ICT state at room temperature and ^3ICT state at 77 K. Since the excited state has ICT character, a Renner–Teller distortion is avoided upon photoexcitation as the metal ion remains effectively in a d^{10} electronic configuration in derivatives with electron-rich aryl ligands. Consequently, the magnitude of k_{nr} is limited to values of 10^6 – 10^7 s^{-1} in fluid solution and decreases further to 10^5 s^{-1} in PS film. This change suggests that the bending distortion is greatly diminished in these ICT emitters.

Table 3. Luminescent properties of complexes **1c** and **2c–g**.

Complex	Room temperature					77 K	
	λ_{em} (nm)	Φ_{PL}	τ (μ s)	k_r (10^5 s $^{-1}$)	k_{nr} (10^5 s $^{-1}$)	λ_{em} (nm)	τ (μ s)
<u>MeTHF</u>							
1c	680	0.002	0.004	5.0	2500	542	83
2c	522	0.12	0.210	5.8	42	432, 456	66
2d	583	0.035	0.083	4.2	120	474	46
2d-Me	594	0.055	0.310	1.8	31	496	63
2e	604	0.013	0.015	8.9	680	496	60
2e-Me	620	0.021	0.128	1.6	76	522	87
<u>MeCy</u>							
1c	586	0.15	0.270	5.4	32	557	86
2c	460	0.004	0.016	2.6	640	436, 456	50
2d	492	0.009	0.052	1.9	190	470	39
2d-Me	520	0.42	3.3	1.3	1.7	508	75
2e	532	0.42	1.6	2.6	3.7	506	53
2e-Me	558	0.35	2.2	1.6	3.0	544	94
<u>1 wt% doped PS film</u>							
1c	620	0.38	0.650	5.8	9.6	612	54
2c	462	0.19	2.3	0.84	3.5	460	41
2d	504	0.28	1.3	2.2	5.5	502	45
2d-Me	520	0.77	4.1	1.9	0.55	526	56
2e	544	0.61	2.5	2.4	1.6	540	65
2e-Me	554	0.61	3.0	2.0	1.3	560	72

The Role of Ligand Rotation in Nonradiative Decay

Even though Renner–Teller distortion is suppressed in the ICT emitters (**1c** and **2c–d**), the luminescence efficiencies remain low in fluid solution and modest even in PS film ($\Phi_{PL} < 0.40$). Other effective nonradiative decay routes must still be present, with a likely candidate involving rotation around the coordinating Au–C_{aryl} and C–N single bonds of the arylamine moiety.²³ The single crystal structures of these complexes show that there are no steric restrictions to rotation of the coordinated phenylene, which may act to increase losses from nonradiative decay. Consistent with this proposal, values for k_{nr} in **1c** and **2c–d** increase as much as two orders of magnitude when measured in fluid solution (MeCy) as opposed to the rigid media of PS (Table 3). Thus, to test this rotational deactivation hypothesis, we prepared complexes **2d**, **2d-Me**, **2e** and **2e-Me**. These complexes have a common MAC carbene acceptor ligand but three different aryl donor ligands. In complex **2d-Me** methyl substituents at the ortho-positions of the coordinated

phenyl ring serve to hinder rotation around the Au–C_{aryl} bond, whereas a julolidine moiety is used to prevent rotation around the C–N bond in **2e**. Finally, ortho-methyl substituents are also introduced to a julolidine moiety in complex **2e-Me**, inhibiting rotation around both the Au–C_{aryl} and C–N bond. (Figure 7)

The effect of the ortho methyl groups on the orientation of the coordinated aryl ligand is evident in the single crystal structures of **2d**, **2d-Me** and **2e-Me**

shown in Figure 8, top. The dihedral angle between the carbene and the aryl ligand in complex **2d** is ~62.5°, comparable to that found in **1c**, which suggests a low energy barrier for rotation around the Au–C_{aryl} bond. In contrast, this dihedral angle is much smaller in complexes **2d-Me** (5.4°) as well as in **2e-Me** (5.8°). The distance between the ortho-methyl carbon to the center of the adjacent phenyl rings in the dipp moieties is between 3.57–3.65 Å in **2d-Me** and 3.57–3.82 Å in **2e-Me**. This separation places these substituents well within the Van der Waals radii of the methyl group (2.0 Å).²⁴ As revealed in space-filling diagrams (Figure 8, bottom), confinement of the two ortho-methyl groups inside the steric shield of the isopropyl groups of the dipp substituents enforces a coplanar geometry between the ligands. This orientation is also evidenced by the chemical shifts of the ortho-methyl signals in the ¹H NMR spectra. Resonances for the ortho-methyl groups in the free ligands *N,N*-3,5-tetramethyl aniline ($\delta = 2.21$ ppm) and 3,5-dimethyl julolidine ($\delta = 2.03$ ppm) shift upfield in **2e-Me** ($\delta = 1.35$ ppm) and **2e-Me** ($\delta = 1.24$ ppm). These shifts suggest that the methyl substituents experience a shielding influence from being pointed toward the center of the phenyl rings of dipp moieties, thus indicating a molecular configuration in fluid solution close to that found in single crystals. To further evaluate whether the rotation around the Au–C_{aryl} bond is hindered by the ortho-methyl substituents, DFT calculations were carried out to scan the molecular potential energy at

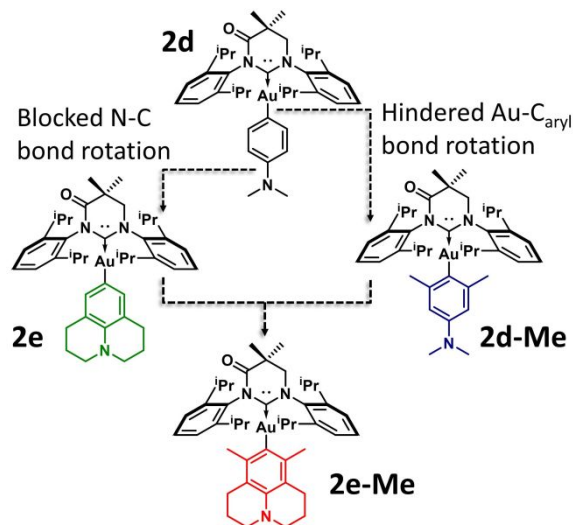


Figure 7. Molecular structure and design strategy for restricted rotation.

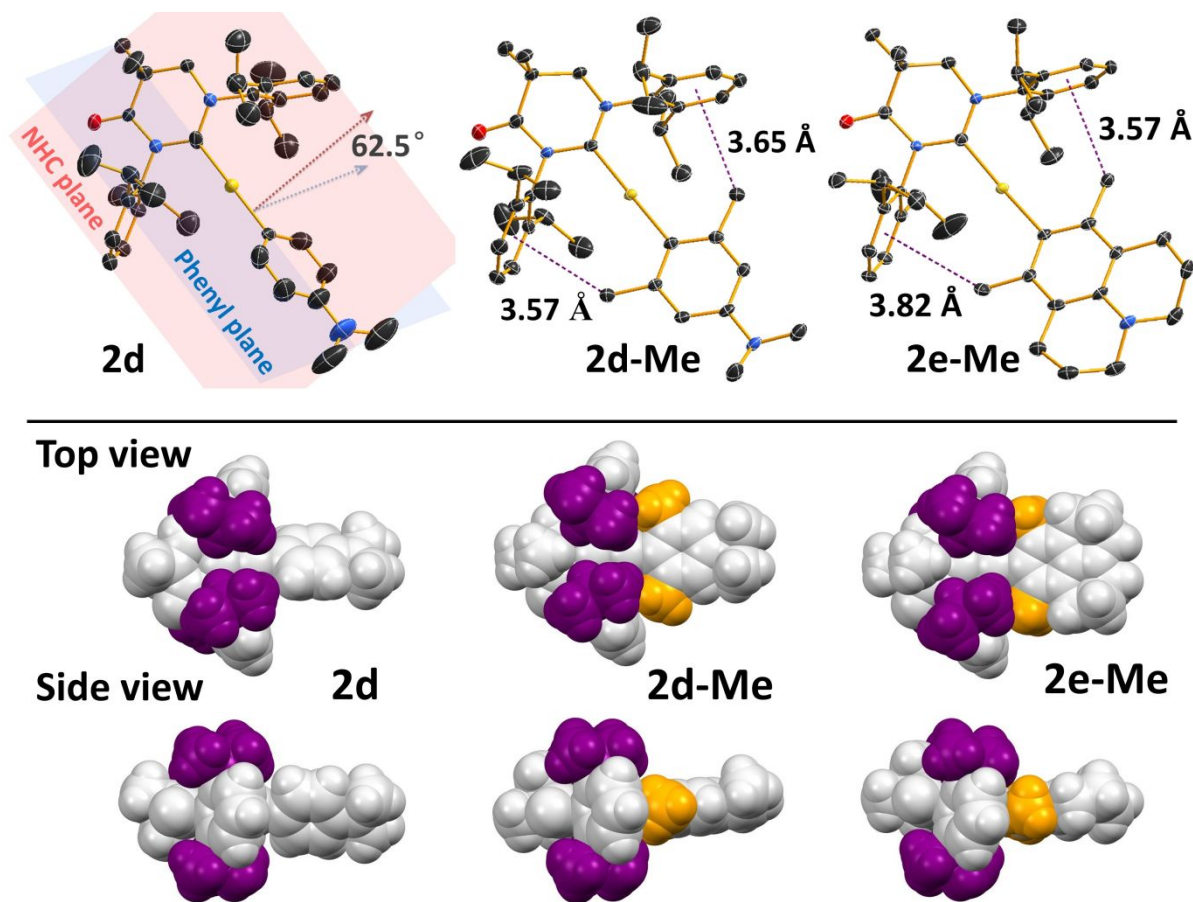


Figure 8. (top) Single crystal thermal ellipsoid diagrams of complex **2d**, **2d-Me** and **2e-Me**, all the non-H atoms are plotted at 50% probability ellipsoid (C: black; N: blue; O: red; Au: gold). H atoms are omitted for clarity; (bottom) space-filling diagrams, the isopropyl moieties are highlighted in purple and the ortho-methyl groups in orange.

different ligand conformations (Figure 9). With the arrangement of the carbene and aryl ligands varied from coplanar (dihedral angle = 0°) to perpendicular (dihedral angle = 90°), energetic barriers for unsubstituted **2d** and **2e** peak at around 2 kcal/mol, whereas the barriers are increased by 4.0 kcal/mol in **2d-Me** and **2e-Me**.

Thus, it is inferred that rotation around the Au-C_{aryl} bond can occur at rates competitive

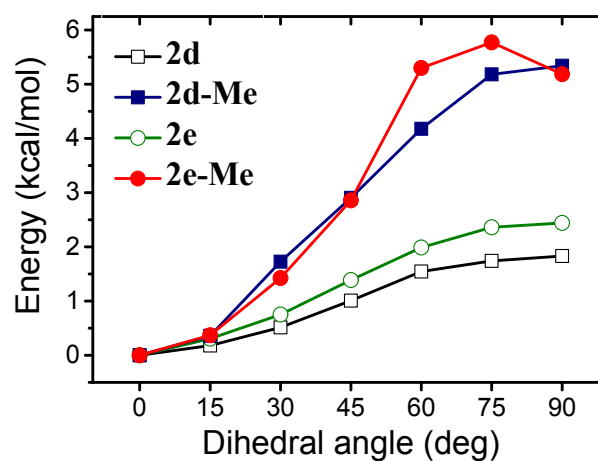


Figure 9. Theoretically calculated molecular energy of **2d/2d-Me** and **2e/2e-Me** with dihedral angle between carbene and aryl moieties varied from 0 to 90° .

with radiative decay in **2d** and **2e**, whereas the ligands in **2d-Me** and **2e-Me** maintain a coplanar molecular geometry within the microsecond lifetimes of their respective excited states.

The oxidation potentials for **2e** and **2e-Me** are cathodically shifted compared with **2d** and **2d-Me** owing to the stronger electron donating strength of the julolidine moiety and *ortho*-methyl groups (Table 1). The electrochemical reduction of complexes **2d-Me** and **2e/2e-Me** are shifted outside of the observable electrochemical window. These derivatives are expected to be ICT emitters due to strong electron donation from the amine-modified aryl ligands. Results

from TD-DFT calculations carried out for complexes **2d/2d-Me** and **2e/2e-Me** are summarized in Table 2. Their optimized geometries in the lowest T_1 state remain linear, indicating that Renner–Teller distortion is avoided (see ESI). Absorption spectra of **2d/2d-Me** and **2e/2e-Me** recorded in dilute cyclohexane solution are shown in Figure 10a.

Intense bands at high energy ($\lambda < 325$ nm) are assigned to π - π^* transitions on the ligands, whereas broad bands at longer wavelengths are attributed to the spin-allowed ICT absorptions. A plot of the oxidation potential versus the onset energy of these low energy bands follows

a linear relationship (see inset in Figure 10a), which supports the ICT character of these transitions where the acceptor is the carbene ligand. Notably, the ICT bands of **2d-Me** and

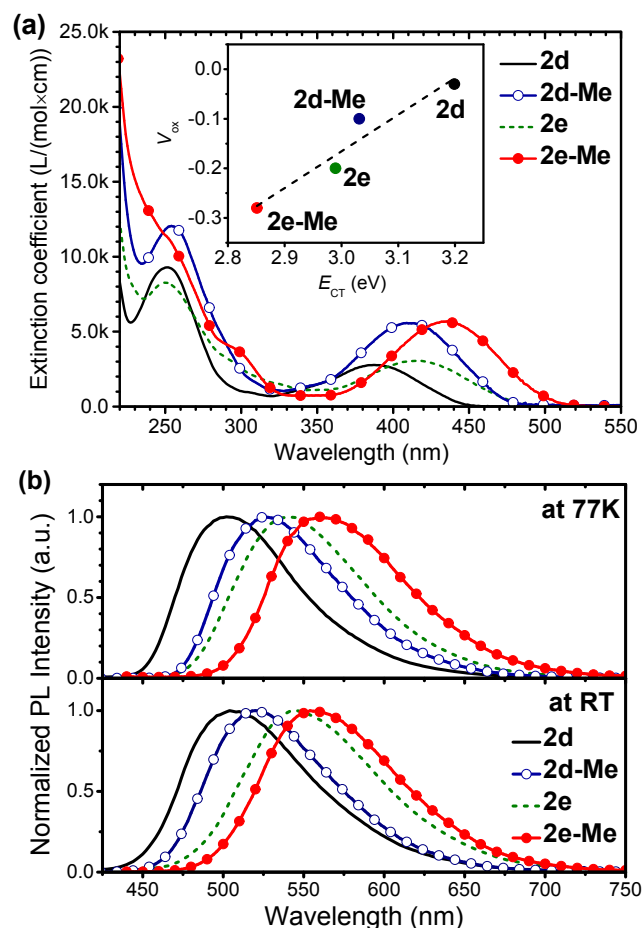


Figure 10. (a) Absorption spectra of complexes **2d/2d-Me** and **2e/2e-Me** in cyclohexane solution at room temperature. Inset: correlation of the low-energy band energy (E_{CT} , determined by the peak maxima) and the oxidation potential (V_{ox} obtained from DPV measurement); (b) Emission spectra of complexes **2d/2d-Me** and **2e/2e-Me** at RT and at 77 K in 1 wt% doped PS film.

1
2
3 **2e-Me** have extinction coefficients ($\epsilon > 5500 \text{ L}/(\text{mol}\times\text{cm})$) almost double those of **2d** and **2e** (ϵ
4 $\sim 3000 \text{ L}/(\text{mol}\times\text{cm})$). A coplanar configuration enhances overlap between the ligand π orbitals in **2d-Me**
5 and **2e-Me** and is reflected by the extinction coefficients of their ICT transition being higher than **2d** and
6 **2e**.

7
8
9
10
11
12 The luminescent properties of complexes **2d-Me** and **2e/2e-Me** were recorded in both solution and PS
13 film (Figure 10b and ESI) and summarized in Table 3. The complexes display broad, featureless emission
14 bands in both MeCy solution and the polymer matrix consistent with an ICT character for the emissive
15 excited state. Consequently, luminescence from **2d-Me** and **2e/2e-Me** displays solvatochromic and
16 rigidochromic behavior similar to that observed for **2c-d** in solution with different polarities and
17 temperature (see SI). An important difference in **2d-Me** and **2e/2e-Me** is a dramatic increase of nearly two
18 orders of magnitude in luminescent efficiency in fluid solution ($\Phi_{\text{PL}} \approx 0.40$) compared to their unconstrained
19 derivatives (**2c-d**). This increase does not come about from a change in the radiative rate constants as
20 values for **2d-Me** and **2e/2e-Me** in MeCy solution ($k_r = 1.3\text{--}2.6 \times 10^5 \text{ s}^{-1}$) are similar to those of **2c-d**,
21 consistent with a Strickler–Berg analysis of their respective absorption spectra (see the ESI). Instead, the
22 high efficiency of **2d-Me** and **2e/2e-Me** in MeCy is due to a corresponding decrease in the rate of
23 nonradiative decay. Since nonradiative decay attributed to Renner–Teller distortion is absent in **2d-Me** and
24 **2e/2e-Me** as ICT emitters, the decrease in k_{nr} is ascribed to restricted rotation of the amine in **2e** and the
25 aryl ligand in **2d-Me/2e-Me** around the C–N and Au–C_{aryl} single bonds. A further increase in quantum
26 efficiency, up to 0.77 for **2d-Me**, is achieved upon dispersing in PS film and is caused by an additional
27 decrease in k_{nr} in the rigid media.

28
29
30
31
32
33
34
35
36
37
38
39
40
41
42
43
44
45
46
47 Informed with the photophysical data above, a semilog plot of k_{nr} versus emission energy in PS for the
48 complexes with ICT emissive states is shown in Figure 11. Compounds that share common promoting
49 vibrational modes which couple the excited and ground states will have values for k_{nr} that increase
50 exponentially with decreasing emission energy (Energy Gap Law).²⁵ Deviations from this behavior are
51 indicative of a change in the vibrational/rotational mechanism responsible for nonradiative decay. Taking
52
53
54
55
56
57

as a reference the known analog having a carbazole donor [(MAC)Au(Cz)], the fastest k_{nr} is found for the complex with lowest emission energy (**1c**). The high k_{nr} for this complex is likely due to effects from vibronic coupling in addition to bond rotation. Notably, complexes **2c** and **2d**, despite having higher emission energies, also have higher k_{nr} values than (MAC)Au(Cz), which emphasizes the effects of excited state deactivation via bond rotation of the aryl ligand. A significant decrease in k_{nr} is found in complex **2d-Me** with hindered rotation along Au–C_{aryl} bond. Finally, complexes **2e** and **2e-Me** have k_{nr} values comparable to (MAC)Au(Cz) even though these aryl derivatives have lower emission energies. Such results indicate that molecular design to restrict rotation of the aryl ligand can effectively decrease energy loss from nonradiative decay in these two coordinate (carbene)Au(aryl) ICT emitters.

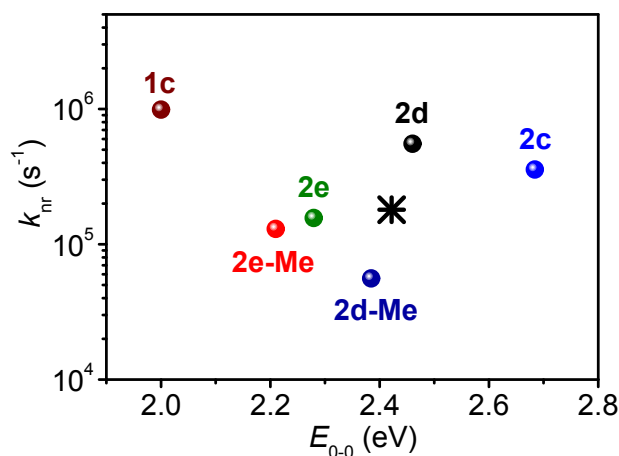


Figure 11. Semilog plot of k_{nr} versus the emission energy for complexes **1c**, **2c–e**, **2d-Me** and **2e-Me** (using data in PS film). The value reported for (MAC)Au(carbazole) is marked with a black star.^{1a}

Temperature dependence of TADF

Luminescent decay lifetimes of all of the (carbene)Au(aryl) ICT emitters in PS film vary within 0.65–4.1 μ s at room temperature yet increase to 42–72 μ s at 77 K. This large change with temperature is consistent thermal activation from triplet to singlet states that is the hallmark of TADF behavior. Thus, transient emission decays were recorded between 77–310 K to further characterize these photophysical processes. A representative example of the emission lifetime plotted as a function of temperature is shown for **2e-Me** in Figure 12; similar plots for **1c**, **2c**, **2d/2d-Me** and **2e** are shown in the ESI. Emission from all of these complexes at low temperature is governed by a long-lived phosphorescence from ³ICT ($T_1 \rightarrow S_0$, >

1
2
3 99%). With increasing temperature, endothermic ISC from T_1 to S_1 is promoted and the radiative decay
4 from S_1 becomes dominant ($> 90\%$), resulting in a drastically decreased lifetime (see ESI for the ratio of
5 phosphorescence vs. TADF). Since luminescence from these emitters decays monoexponentially in the
6 measured temperature range, it is inferred that thermal equilibrium is established well before either
7 phosphorescence or TADF because of the fast rate for ISC in these types of complexes.^{3c, 26} Therefore, two
8 Boltzmann distribution models were employed to fit the temperature-dependent lifetime curves as
9 illustrated in Figure 12.^{1a, 1c} The two-level model assumes only S_1 and T_1 states having an energy gap of
10 ΔE_{ST} , whereas the three-level model takes into consideration zero-field-splitting (ZFS) of the triplet
11 sublevels. Both models provide the same trends for the exchange energy ΔE_{ST} , but the three-level model
12 gives a better fit in the low temperature regime. Kinetic and thermodynamic parameters derived from the
13 photophysical measurements using the three-level model are given in Table 4. Data from these fits show
14 the smallest ΔE_{ST} in **1c** (686 cm^{-1} , 85.0 meV) and largest in **2c** (1640 cm^{-1} , 203 meV), whereas **2d/2d-Me**
15 and **2e/2e-Me** have comparable values ranging between 1120 cm^{-1} (139 meV) and 1280 cm^{-1} (159 meV).
16 The ZFS values derived from the three-level model exceed 130 cm^{-1} (except for **1c**, ZFS = 11 cm^{-1}) and are
17 comparable to values previously reported two coordinate (carbene)M(carbazole) complexes.^{1a, 1c} Such
18 impressive ZFS effects explain the poor fits of the two-level model at low temperature. However, it should
19 be noted that the values given for the ZFS in Table 4 are somewhat unreliable as large fitting errors can be
20 generated due to the paucity of data collected at temperatures where the effects of ZFS are most pronounced
21 ($<120\text{ K}$).
22
23
24
25
26
27
28
29
30
31
32
33
34
35
36
37
38
39
40
41
42
43
44
45
46
47
48
49
50
51
52
53
54
55
56
57
58
59
60

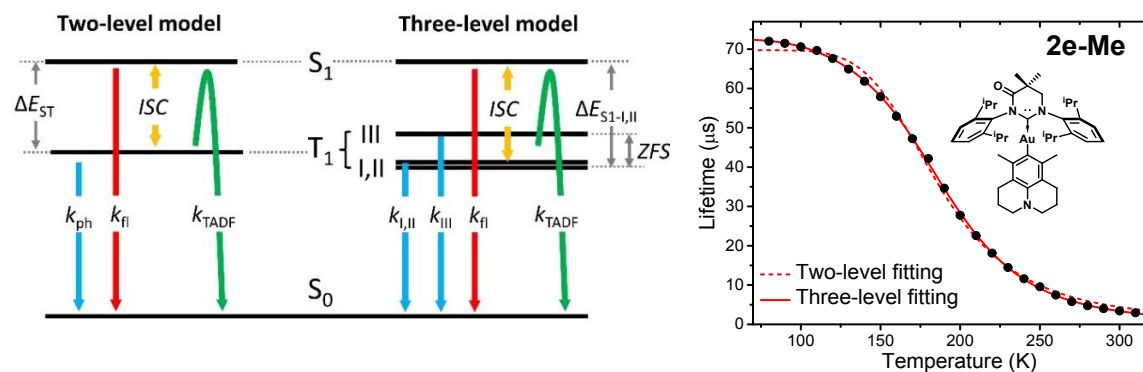


Figure 12. Two-level and three-level models for the description of emission in (carbene)Au(aryl) complexes (the fitting equations are given in the previous report^{1a}) and the temperature-dependent lifetime of **2e-Me** in PS film with fitting curves.

Table 4. Photophysical data derived from three-level Boltzmann fits to temperature-dependent lifetimes

Complex	ΔE_{ST} (cm ⁻¹)	ZFS (cm ⁻¹)	τ_{fl} (ns)	$\tau_{I,II}$ (μ s)	τ_{III} (μ s)
1c	690	11	14	68	34
2c	1600	290	0.53	44	5.7
2d	1300	600	2.9	45	0.30
2d-Me	1200	230	7.0	57	20
2e	1100	140	5.9	71	22
2e-Me	1200	420	4.7	73	3.1

Conclusion

The work presented here shows (carbene)Au(aryl) complexes are promising chromophores for luminescent applications. These two coordinate (carbene)Au(aryl) complexes can be prepared using readily accessible aryl boronic acids or pinacol esters. Their emission color is tuned from sky blue to red by changing carbene ligand and electron donation strength of the substituent on the aryl ligand. A bending distortion is expected upon excitation in species with an MLCT excited state, owing to transient oxidation of the Au center from d¹⁰ to d⁹, referred to as the Renner-Teller effect. However, by increasing the electron donating strength of the substituent on the phenyl ligand, the energy of the aryl π electrons can be raised above that of the Au d electrons. Consequently, the excited state alignment can be tuned, and the lowest excited state character changed from MLCT to ICT. Single crystal X-ray analysis shows that rotation

1
2
3 around the Au–C_{aryl} and amine C–N bond is unencumbered and expected to be facile. The conformational
4 flexibility of aryl ligands can be restricted by chemical modifications, such as introducing ortho-methyl
5 groups or the julolidine moiety. Increasing the molecular rigidity by restricting single bond rotation
6 improves the luminescence efficiency by further decreasing the rate of nonradiative decay.
7
8
9
10

11
12 These two-coordinate complexes provide new models for investigation of dynamic change of molecular
13 geometry in the excited state and are complementary to three- and four-coordinated d¹⁰ chromophores that
14 distort in the excited state via the Jahn-Teller effect. It is noteworthy that the luminescent properties of these
15 two-coordinate complexes with ICT emission are comparable to the recently reported four-coordinate d⁸
16 Au TADF derivatives where the metal center is in a formal Au(III) oxidation state.^{6c} The similarity in
17 photophysical properties supports the assumption that oxidation of the formally Au(I) metal center does not
18 occur upon excitation in (carbene)Au(aryl) complexes with ICT emissive states. This work highlights the
19 importance of avoiding a situation where the lowest excited state with MLCT character when aiming for
20 highly luminescent candidates in metals with d¹⁰ electronic configurations since the geometric distortion
21 opens up efficient nonradiative decay pathways. Enhanced quantum yields are therefore observed in
22 complexes that have lowest energy excited states with ICT character, where the Au center is free from
23 transient oxidation, and which keeps the excited molecules in geometries similar to the ground state. Our
24 (carbene)Au(aryl) complexes thus enrich the library of the luminescent coinage metal complexes, providing
25 additional opportunities to discover new photodynamic and optoelectronic properties.
26
27
28
29
30
31
32
33
34
35
36
37
38
39
40

41 42 **Acknowledgment**

43
44
45 This work was supported by the Universal Display Corporation.
46
47

48 **Supporting Information**

49
50 Detailed synthetic procedures and characterization; NMR spectra; single crystal X-ray diffraction data; CV
51 and DPV curves; photophysical data including temperature-dependent lifetime measurements and data
52 from theoretical calculations.
53
54
55
56
57
58
59
60

1
2
3 **Author Information**
4

5
6 Corresponding Authors

7
8 Mark E. Thompson – *University of Southern California, Los Angeles, California*; orcid.org/0000-0002-
9 7764-4096.

10
11
12 E-mail: met@usc.edu
13

14 Other Authors

15
16 Tian-yi Li – *University of Southern California, Los Angeles, California*; orcid.org/0000-0003-4247-5840

17
18 Daniel Sylvinson Muthiah Ravinson – *University of Southern California, Los Angeles, California*

19
20 Ralf Haiges – *University of Southern California, Los Angeles, California*; orcid.org/0000-0003-4151-3593

21
22
23 Peter I. Djurovich – *University of Southern California, Los Angeles, California*; orcid.org/0000-0001-6716-
24 389X
25
26
27
28
29
30
31
32
33
34
35
36
37
38
39
40
41
42
43
44
45
46
47
48
49
50
51
52
53
54
55
56
57
58
59
60

References

1. (a) Hamze, R.; Shi, S.; Kapper, S. C.; Muthiah Ravinson, D. S.; Estergreen, L.; Jung, M.-C.; Tadle, A. C.; Haiges, R.; Djurovich, P. I.; Peltier, J. L.; Jazzar, R.; Bertrand, G.; Bradforth, S. E.; Thompson, M. E., "Quick-Silver" from a Systematic Study of Highly Luminescent, Two-Coordinate, D10 Coinage Metal Complexes. *Journal of the American Chemical Society* **2019**, *141* (21), 8616-8626, DOI: 10.1021/jacs.9b03657;
 - (b) Hamze, R.; Peltier, J. L.; Sylvinson, D.; Jung, M.; Cardenas, J.; Haiges, R.; Soleilhavoup, M.; Jazzar, R.; Djurovich, P. I.; Bertrand, G.; Thompson, M. E., Eliminating Nonradiative Decay in Cu(I) Emitters: >99% Quantum Efficiency and Microsecond Lifetime. *Science* **2019**, *363* (6427), 601, DOI: 10.1126/science.aav2865;
 - (c) Shi, S.; Jung, M. C.; Coburn, C.; Tadle, A.; Sylvinson M. R, D.; Djurovich, P. I.; Forrest, S. R.; Thompson, M. E., Highly Efficient Photo- and Electroluminescence from Two-Coordinate Cu(I) Complexes Featuring Nonconventional N-Heterocyclic Carbenes. *Journal of the American Chemical Society* **2019**, *141* (8), 3576-3588, DOI: 10.1021/jacs.8b12397;
 - (d) Romanov, A. S.; Yang, L.; Jones, S. T. E.; Di, D.; Morley, O. J.; Drummond, B. H.; Reponen, A. P. M.; Linnolahti, M.; Credgington, D.; Bochmann, M., Dendritic Carbene Metal Carbazole Complexes as Photoemitters for Fully Solution-Processed Oleds. *Chemistry of Materials* **2019**, *31* (10), 3613-3623, DOI: 10.1021/acs.chemmater.8b05112;
 - (e) Bachmann, M.; Fessler, R.; Blacque, O.; Venkatesan, K., Towards Blue Emitting Monocyclometalated Gold(III) Complexes - Synthesis, Characterization and Photophysical Investigations. *Dalton Transactions* **2019**, *48* (21), 7320-7330, DOI: 10.1039/c8dt05034a;
 - (f) Romanov, A. S.; Jones, S. T. E.; Yang, L.; Conaghan, P. J.; Di, D.; Linnolahti, M.; Credgington, D.; Bochmann, M., Mononuclear Silver Complexes for Efficient Solution and Vacuum-Processed Oleds. *Advanced Optical Materials* **2018**, *6* (24), 1801347, DOI: doi:10.1002/adom.201801347;
 - (g) Conaghan, P. J.; Menke, S. M.; Romanov, A. S.; Jones, S. T. E.; Pearson, A. J.; Evans, E. W.; Bochmann, M.; Greenham, N. C.; Credgington, D., Efficient Vacuum-Processed Light-Emitting Diodes Based on Carbene-Metal-Amides. *Advanced Materials* **2018**, *30* (35), 1802285, DOI: 10.1002/adma.201802285;
 - (h) Di, D.; Romanov, A. S.; Yang, L.; Richter, J. M.; Rivett, J. P. H.; Jones, S.; Thomas, T. H.; Abdi Jalebi, M.; Friend, R. H.; Linnolahti, M.; Bochmann, M.; Credgington, D., High-Performance Light-Emitting Diodes Based on Carbene-Metal-Amides. *Science* **2017**, *356* (6334), 159, DOI: 10.1126/science.aah4345;
 - (i) Yam, V. W. W.; Lee, J. K. W.; Ko, C. C.; Zhu, N. Y., Photochromic Diarylethene-Containing Ionic Liquids and N-Heterocyclic Carbenes. *Journal of the American Chemical Society* **2009**, *131* (3), 912-+, DOI: 10.1021/ja808791e
-
2. (a) Tanaka, H.; Shizu, K.; Miyazaki, H.; Adachi, C., Efficient Green Thermally Activated Delayed Fluorescence (TADF) from a Phenoxazine-Triphenyltriazine (Pxz-Trz) Derivative. *Chemical Communications* **2012**, *48* (93), 11392-11394, DOI: 10.1039/c2cc36237f;
 - (b) Zhang, Q.; Kuwabara, H.; Potsavage, W. J.; Huang, S.; Hatae, Y.; Shibata, T.; Adachi, C., Anthraquinone-Based Intramolecular Charge-Transfer Compounds: Computational Molecular Design, Thermally Activated Delayed Fluorescence, and Highly Efficient Red Electroluminescence. *Journal of the American Chemical Society* **2014**, *136* (52), 18070-18081, DOI: 10.1021/ja510144h;
 - (c) Rajamalli, P.; Senthilkumar, N.; Gandeepan, P.; Huang, P.-Y.; Huang, M.-J.; Ren-Wu, C.-Z.; Yang, C.-Y.; Chiu, M.-J.; Chu, L.-K.; Lin, H.-W.; Cheng, C.-H., A New Molecular Design Based on Thermally Activated Delayed Fluorescence for Highly Efficient Organic Light Emitting Diodes. *Journal of the American Chemical Society* **2016**, *138* (2), 628-634, DOI: 10.1021/jacs.5b10950;

(d) Tanaka, H.; Shizu, K.; Nakanotani, H.; Adachi, C., Twisted Intramolecular Charge Transfer State for Long-Wavelength Thermally Activated Delayed Fluorescence. *Chemistry of Materials* **2013**, *25* (18), 3766-3771, DOI: 10.1021/cm402428a;

(e) Im, Y.; Kim, M.; Cho, Y. J.; Seo, J.-A.; Yook, K. S.; Lee, J. Y., Molecular Design Strategy of Organic Thermally Activated Delayed Fluorescence Emitters. *Chemistry of Materials* **2017**, *29* (5), 1946-1963, DOI: 10.1021/acs.chemmater.6b05324;

(f) Ahn, D. H.; Kim, S. W.; Lee, H.; Ko, I. J.; Karthik, D.; Lee, J. Y.; Kwon, J. H., Highly Efficient Blue Thermally Activated Delayed Fluorescence Emitters Based on Symmetrical and Rigid Oxygen-Bridged Boron Acceptors. *Nature Photonics* **2019**, *13* (8), 540-546, DOI: 10.1038/s41566-019-0415-5;

(g) Li, P.; Chan, H.; Lai, S.-L.; Ng, M.; Chan, M.-Y.; Yam, V. W.-W., Four-Coordinate Boron Emitters with Tridentate Chelating Ligand for Efficient and Stable Thermally Activated Delayed Fluorescence Organic Light-Emitting Devices. *Angewandte Chemie International Edition* **2019**, *58* (27), 9088-9094, DOI: 10.1002/anie.201903332

3. (a) Föllner, J.; Marian, C. M., Rotationally Assisted Spin-State Inversion in Carbene–Metal–Amides Is an Artifact. *The Journal of Physical Chemistry Letters* **2017**, *8* (22), 5643-5647, DOI: 10.1021/acs.jpcclett.7b02701;

(b) Taffet, E. J.; Olivier, Y.; Lam, F.; Beljonne, D.; Scholes, G. D., Carbene–Metal–Amide Bond Deformation, Rather Than Ligand Rotation, Drives Delayed Fluorescence. *The Journal of Physical Chemistry Letters* **2018**, *9* (7), 1620-1626, DOI: 10.1021/acs.jpcclett.8b00503;

(c) Hall, C. R.; Romanov, A. S.; Bochmann, M.; Meech, S. R., Ultrafast Structure and Dynamics in the Thermally Activated Delayed Fluorescence of a Carbene–Metal–Amide. *The Journal of Physical Chemistry Letters* **2018**, *9* (19), 5873-5876, DOI: 10.1021/acs.jpcclett.8b02797

4. (a) Hung, F.-F.; To, W.-P.; Zhang, J.-J.; Ma, C.; Wong, W.-Y.; Che, C.-M., Water-Soluble Luminescent Cyclometalated Gold(III) Complexes with Cis-Chelating Bis(N-Heterocyclic Carbene) Ligands: Synthesis and Photophysical Properties. *Chemistry – A European Journal* **2014**, *20* (28), 8604-8614, DOI: 10.1002/chem.201403103;

(b) Malmberg, R.; Bachmann, M.; Blacque, O.; Venkatesan, K., Thermally Robust and Tuneable Phosphorescent Gold(III) Complexes Bearing (N^N)-Type Bidentate Ligands as Ancillary Chelates. *Chemistry-A European Journal* **2019**, *25* (14), 3627-3636, DOI: 10.1002/chem.201805486;

(c) von Arx, T.; Szentkuti, A.; Zehnder, T. N.; Blacque, O.; Venkatesan, K., Stable N-Heterocyclic Carbene (Nhc) Cyclometalated (C₆) Gold(III) Complexes as Blue-Green Phosphorescence Emitters. *Journal of Materials Chemistry C* **2017**, *5* (15), 3765-3769, DOI: 10.1039/c6tc05551f;

(d) Garg, J. A.; Blacque, O.; Fox, T.; Venkatesan, K., Stable and Tunable Phosphorescent Neutral Cyclometalated Au(III) Diaryl Complexes. *Inorganic Chemistry* **2010**, *49* (24), 11463-11472, DOI: 10.1021/ic101437h

5. (a) Yam, V. W.-W.; Wong, K. M.-C.; Hung, L.-L.; Zhu, N., Luminescent Gold(III) Alkynyl Complexes: Synthesis, Structural Characterization, and Luminescence Properties. *Angewandte Chemie International Edition* **2005**, *44* (20), 3107-3110, DOI: 10.1002/anie.200500253;

(b) Wong, K. M.-C.; Hung, L.-L.; Lam, W. H.; Zhu, N.; Yam, V. W.-W., A Class of Luminescent Cyclometalated Alkynylgold(III) Complexes: Synthesis, Characterization, and Electrochemical, Photophysical, and Computational Studies of [Au(C₆H₄N₂C)(C₆H₄N₂C)] (C₆H₄N₂C = K₃c,N,C Bis-Cyclometalated 2,6-Diphenylpyridyl). *Journal of the American Chemical Society* **2007**, *129* (14), 4350-4365, DOI: 10.1021/ja068264u;

(c) Au, V. K.-M.; Wong, K. M.-C.; Tsang, D. P.-K.; Chan, M.-Y.; Zhu, N.; Yam, V. W.-W., High-Efficiency Green Organic Light-Emitting Devices Utilizing Phosphorescent Bis-Cyclometalated

Alkynylgold(III) Complexes. *Journal of the American Chemical Society* **2010**, *132* (40), 14273-14278, DOI: 10.1021/ja106579d;

(d) Tang, M.-C.; Tsang, D. P.-K.; Chan, M. M.-Y.; Wong, K. M.-C.; Yam, V. W.-W., Dendritic Luminescent Gold(III) Complexes for Highly Efficient Solution-Processable Organic Light-Emitting Devices. *Angewandte Chemie International Edition* **2013**, *52* (1), 446-449, DOI: 10.1002/anie.201206457;

(e) Au, V. K.-M.; Wu, D.; Yam, V. W.-W., Organic Memory Devices Based on a Bis-Cyclometalated Alkynylgold(III) Complex. *Journal of the American Chemical Society* **2015**, *137* (14), 4654-4657, DOI: 10.1021/jacs.5b02113;

(f) Tang, M.-C.; Lee, C.-H.; Lai, S.-L.; Ng, M.; Chan, M.-Y.; Yam, V. W.-W., Versatile Design Strategy for Highly Luminescent Vacuum-Evaporable and Solution-Processable Tridentate Gold(III) Complexes with Monoaryl Auxiliary Ligands and Their Applications for Phosphorescent Organic Light Emitting Devices. *Journal of the American Chemical Society* **2017**, *139* (27), 9341-9349, DOI: 10.1021/jacs.7b04788;

(g) Tang, M.-C.; Lee, C.-H.; Ng, M.; Wong, Y.-C.; Chan, M.-Y.; Yam, V. W.-W., Highly Emissive Fused Heterocyclic Alkynylgold(III) Complexes for Multiple Color Emission Spanning from Green to Red for Solution-Processable Organic Light-Emitting Devices. *Angewandte Chemie International Edition* **2018**, *57* (19), 5463-5466, DOI: 10.1002/anie.201711846;

(h) Li, L.-K.; Tang, M.-C.; Lai, S.-L.; Ng, M.; Kwok, W.-K.; Chan, M.-Y.; Yam, V. W.-W., Strategies Towards Rational Design of Gold(III) Complexes for High-Performance Organic Light-Emitting Devices. *Nature Photonics* **2019**, *13* (3), 185-191, DOI: 10.1038/s41566-018-0332-z

6. (a) Zhou, D. L.; To, W. P.; Kwak, Y.; Cho, Y.; Cheng, G.; Tong, G. S. M.; Che, C. M., Thermally Stable Donor-Acceptor Type (Alkynyl)Gold(III) TADF Emitters Achieved EQEs and Luminance of up to 23.4% and 70 300 Cd M⁻² in Vacuum-Deposited OLEDs. *Advanced Science* **2019**, *6* (18), DOI: 10.1002/advs.201802297;

(b) Tang, M.-C.; Leung, M.-Y.; Lai, S.-L.; Ng, M.; Chan, M.-Y.; Wing-Wah Yam, V., Realization of Thermally Stimulated Delayed Phosphorescence in Arylgold(III) Complexes and Efficient Gold(III) Based Blue-Emitting Organic Light-Emitting Devices. *Journal of the American Chemical Society* **2018**, *140* (40), 13115-13124, DOI: 10.1021/jacs.8b09205;

(c) To, W.-P.; Zhou, D.; Tong, G. S. M.; Cheng, G.; Yang, C.; Che, C.-M., Highly Luminescent Pincer Gold(III) Aryl Emitters: Thermally Activated Delayed Fluorescence and Solution-Processed OLEDs. *Angewandte Chemie International Edition* **2017**, *56* (45), 14036-14041, DOI: 10.1002/anie.201707193

7. (a) Lopez-de-Luzuriaga, J. M.; Monge, M.; Olmos, M. E., Luminescent Aryl-Group Eleven Metal Complexes. *Dalton Transactions* **2017**, *46* (7), 2046-2067, DOI: 10.1039/c6dt04386k;

(b) Mihaly, J. J.; Stewart, D. J.; Grusenmeyer, T. A.; Phillips, A. T.; Haley, J. E.; Zeller, M.; Gray, T. G., Photophysical Properties of Organogold(I) Complexes Bearing a Benzothiazole-2,7-Fluorenyl Moiety: Selection of Ancillary Ligand Influences White Light Emission. *Dalton Transactions* **2019**, *48* (42), 15917-15927, DOI: 10.1039/c9dt02312g;

(c) Molteni, R.; Edkins, K.; Haehnel, M.; Steffen, A., C-H Activation of Fluoroarenes: Synthesis, Structure, and Luminescence Properties of Copper(I) and Gold(I) Complexes Bearing 2-Phenylpyridine Ligands. *Organometallics* **2016**, *35* (5), 629-640, DOI: 10.1021/acs.organomet.5b00904;

(d) Gao, L.; Niedzwiecki, D. S.; Deligonul, N.; Zeller, M.; Hunter, A. D.; Gray, T. G., Gold(I) Styrylbenzene, Distyrylbenzene, and Distyrylnaphthalene Complexes: High Emission Quantum Yields at Room Temperature. *Chemistry-A European Journal* **2012**, *18* (20), 6316-6327, DOI: 10.1002/chem.201102502;

(e) Gao, L.; Peay, M. A.; Partyka, D. V.; Updegraff, J. B.; Teets, T. S.; Esswein, A. J.; Zeller, M.; Hunter, A. D.; Gray, T. G., Mono- and Di-Gold(I) Naphthalenes and Pyrenes: Syntheses, Crystal Structures, and Photophysics. *Organometallics* **2009**, *28* (19), 5669-5681, DOI: 10.1021/om9005214;

(f) Partyka, D. V.; Esswein, A. J.; Zeller, M.; Hunter, A. D.; Gray, T. G., Gold(I) Pyrenyls: Excited-State Consequences of Carbon-Gold Bond Formation. *Organometallics* **2007**, *26* (14), 3279-3282, DOI: 10.1021/om700346v;

(g) Wing-Wah Yam, V.; Cheung, K.-L.; Yip, S.-K.; Zhu, N., Synthesis, Characterisation, Electrochemistry and Luminescence Studies of 9-Anthrylgold(I) Complexes. *Photochemical & Photobiological Sciences* **2005**, *4* (1), 149-153, DOI: 10.1039/b410667a

8. (a) Guyon, F.; Hameau, A.; Khatyr, A.; Knorr, M.; Amrouche, H.; Fortin, D.; Harvey, P. D.; Strohmman, C.; Ndiaye, A. L.; Huch, V.; Veith, M.; Avarvari, N., Syntheses, Structures, and Photophysical Properties of Mono- and Dinuclear Sulfur-Rich Gold(I) Complexes. *Inorganic Chemistry* **2008**, *47* (17), 7483-7492, DOI: 10.1021/ic7022067;

(b) Yam, V. W. W.; Lo, K. K. W., Luminescent Polynuclear D¹⁰ Metal Complexes. *Chemical Society Reviews* **1999**, *28* (5), 323-334, DOI: 10.1039/a804249g;

(c) Rawashdeh-Omary, M. A.; Omary, M. A.; Patterson, H. H.; Fackler, J. P., Excited-State Interactions for Au(Cn)₂^{-N} and Ag(Cn)₂^{-N} Oligomers in Solution. Formation of Luminescent Gold-Gold Bonded Excimers and Exciplexes. *Journal of the American Chemical Society* **2001**, *123* (45), 11237-11247, DOI: 10.1021/ja011176j;

(d) King, C.; Wang, J. C.; Khan, M. N. I.; Fackler, J. P., Luminescence and Metal-Metal Interactions in Binuclear Gold(I) Compounds. *Inorganic Chemistry* **1989**, *28* (11), 2145-2149, DOI: 10.1021/ic00310a026;

(e) Balch, A. L., Remarkable Luminescence Behaviors and Structural Variations of Two-Coordinate Gold(I) Complexes. In *Photofunctional Transition Metals Complexes*, Yam, V. W. W., Ed. 2007; Vol. 123, pp 1-40;

(f) Chao, H. Y.; Lu, W.; Li, Y. Q.; Chan, M. C. W.; Che, C. M.; Cheung, K. K.; Zhu, N. Y., Organic Triplet Emissions of Arylacetylide Moieties Harnessed through Coordination to Au(Pcy₃)⁺. Effect of Molecular Structure Upon Photoluminescent Properties. *Journal of the American Chemical Society* **2002**, *124* (49), 14696-14706, DOI: 10.1021/ja0209417

9. (a) Hussaini, S. Y.; Haque, R. A.; Li, J. H.; Zhan, S. Z.; Tan, K. W.; Razali, M. R., Coinage Metal Complexes of N-Heterocyclic Carbene Bearing Nitrile Functionalization: Synthesis and Photophysical Properties. *Applied Organometallic Chemistry* **2019**, *33* (6), DOI: 10.1002/aoc.4927;

(b) Vogler, A.; Kunkely, H., Photoreactivity of Gold Complexes. *Coordination Chemistry Reviews* **2001**, *219*, 489-507, DOI: 10.1016/s0010-8545(01)00348-4;

(c) Watase, S.; Nakamoto, M.; Kitamura, T.; Kanehisa, N.; Kai, Y.; Yanagida, S., Solid-State Luminescence and Crystal Structures of Novel Gold(I) Benzenethiolate Complexes. *Journal Of The Chemical Society-Dalton Transactions* **2000**, (20), 3585-3590, DOI: 10.1039/b006572m;

(d) Gao, L.; Partyka, D. V.; Updegraff, J. B.; Deligonul, N.; Gray, T. G., Synthesis, Structures, and Excited-State Geometries of Alkynylgold(I) Complexes. *European Journal of Inorganic Chemistry* **2009**, (18), 2711-2719, DOI: 10.1002/ejic.200900307

10. Bartolomé, C.; Carrasco-Rando, M.; Coco, S.; Cordovilla, C.; Martín-Alvarez, J. M.; Espinet, P., Luminescent Gold(I) Carbenes from 2-Pyridylisocyanide Complexes: Structural Consequences of Intramolecular Versus Intermolecular Hydrogen-Bonding Interactions. *Inorganic Chemistry* **2008**, *47* (5), 1616-1624, DOI: 10.1021/ic702201e

11. (a) Czerwieńec, R.; Yu, J.; Yersin, H., Blue-Light Emission of Cu(I) Complexes and Singlet Harvesting. *Inorganic Chemistry* **2011**, *50* (17), 8293-8301, DOI: 10.1021/ic200811a;

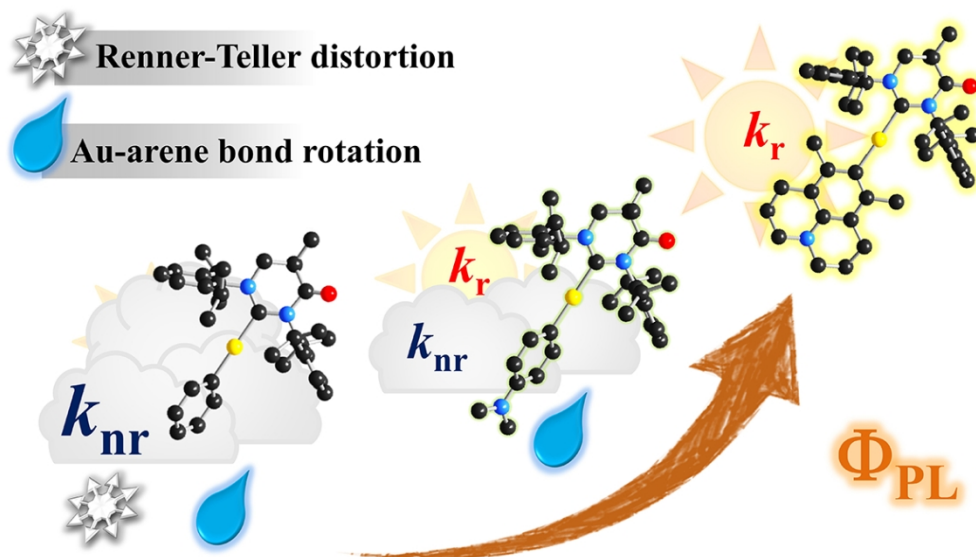
- (b) Hofbeck, T.; Monkowius, U.; Yersin, H., Highly Efficient Luminescence of Cu(I) Compounds: Thermally Activated Delayed Fluorescence Combined with Short-Lived Phosphorescence. *Journal of the American Chemical Society* **2015**, *137* (1), 399-404, DOI: 10.1021/ja5109672;
- (c) Shafikov, M. Z.; Suleymanova, A. F.; Czerwieniec, R.; Yersin, H., Thermally Activated Delayed Fluorescence from Ag(I) Complexes: A Route to 100% Quantum Yield at Unprecedentedly Short Decay Time. *Inorganic Chemistry* **2017**, *56* (21), 13274-13285, DOI: 10.1021/acs.inorgchem.7b02002;
- (d) Yersin, H.; Czerwieniec, R.; Shafikov, M. Z.; Suleymanova, A. F., Tadf Material Design: Photophysical Background and Case Studies Focusing on Cui and Agi Complexes. *Chemphyschem* **2017**, *18* (24), 3508-3535, DOI: 10.1002/cphc.201700872;
- (e) Schinabeck, A.; Leitl, M. J.; Yersin, H., Dinuclear Cu(I) Complex with Combined Bright Tadf and Phosphorescence. Zero-Field Splitting and Spin–Lattice Relaxation Effects of the Triplet State. *The Journal of Physical Chemistry Letters* **2018**, *9* (11), 2848-2856, DOI: 10.1021/acs.jpcclett.8b00957;
- (f) Schinabeck, A.; Chen, J.; Kang, L.; Teng, T.; Homeier, H. H. H.; Suleymanova, A. F.; Shafikov, M. Z.; Yu, R.; Lu, C.-Z.; Yersin, H., Symmetry-Based Design Strategy for Unprecedentedly Fast Decaying Thermally Activated Delayed Fluorescence (Tadf). Application to Dinuclear Cu(I) Compounds. *Chemistry of Materials* **2019**, *31* (12), 4392-4404, DOI: 10.1021/acs.chemmater.9b00671;
- (g) Shafikov, M. Z.; Suleymanova, A. F.; Czerwieniec, R.; Yersin, H., Design Strategy for Ag(I)-Based Thermally Activated Delayed Fluorescence Reaching an Efficiency Breakthrough. *Chemistry of Materials* **2017**, *29* (4), 1708-1715, DOI: 10.1021/acs.chemmater.6b05175;
- (h) Osawa, M.; Kawata, I.; Ishii, R.; Igawa, S.; Hashimoto, M.; Hoshino, M., Application of Neutral D10 Coinage Metal Complexes with an Anionic Bidentate Ligand in Delayed Fluorescence-Type Organic Light-Emitting Diodes. *Journal of Materials Chemistry C* **2013**, *1* (28), 4375-4383, DOI: 10.1039/c3tc30524d;
- (i) Osawa, M.; Hoshino, M.; Hashimoto, M.; Kawata, I.; Igawa, S.; Yashima, M., Application of Three-Coordinate Copper(I) Complexes with Halide Ligands in Organic Light-Emitting Diodes That Exhibit Delayed Fluorescence. *Dalton Transactions* **2015**, *44* (18), 8369-8378, DOI: 10.1039/c4dt02853h;
- (j) Hashimoto, M.; Igawa, S.; Yashima, M.; Kawata, I.; Hoshino, M.; Osawa, M., Highly Efficient Green Organic Light-Emitting Diodes Containing Luminescent Three-Coordinate Copper(I) Complexes. *Journal of the American Chemical Society* **2011**, *133* (27), 10348-10351, DOI: 10.1021/ja202965y

12. (a) Iwamura, M.; Takeuchi, S.; Tahara, T., Ultrafast Excited-State Dynamics of Copper(I) Complexes. *Accounts of Chemical Research* **2015**, *48* (3), 782-791, DOI: 10.1021/ar500353h;
- (b) Iwamura, M.; Takeuchi, S.; Tahara, T., Real-Time Observation of the Photoinduced Structural Change of Bis(2,9-Dimethyl-1,10-Phenanthroline)Copper(I) by Femtosecond Fluorescence Spectroscopy: A Realistic Potential Curve of the Jahn–Teller Distortion. *Journal of the American Chemical Society* **2007**, *129* (16), 5248-5256, DOI: 10.1021/ja069300s;
- (c) Garakyaraghi, S.; Danilov, E. O.; McCusker, C. E.; Castellano, F. N., Transient Absorption Dynamics of Sterically Congested Cu(I) Mlct Excited States. *The Journal of Physical Chemistry A* **2015**, *119* (13), 3181-3193, DOI: 10.1021/acs.jpca.5b00901

13. (a) Barakat, K. A.; Cundari, T. R.; Omary, M. A., Jahn–Teller Distortion in the Phosphorescent Excited State of Three-Coordinate Au(I) Phosphine Complexes. *Journal of the American Chemical Society* **2003**, *125* (47), 14228-14229, DOI: 10.1021/ja036508u;
- (b) Krylova, V. A.; Djurovich, P. I.; Aronson, J. W.; Haiges, R.; Whited, M. T.; Thompson, M. E., Structural and Photophysical Studies of Phosphorescent Three-Coordinate Copper(I) Complexes Supported by an N-Heterocyclic Carbene Ligand. *Organometallics* **2012**, *31* (22), 7983-7993, DOI: 10.1021/om300656v;
- (c) Hamze, R.; Jazzar, R.; Soleilhavoup, M.; Djurovich, P. I.; Bertrand, G.; Thompson, M. E., Phosphorescent 2-, 3- and 4-Coordinate Cyclic (Alkyl)(Amino)Carbene (Caac) Cu(I) Complexes. *Chemical Communications* **2017**, *53* (64), 9008-9011, DOI: 10.1039/c7cc02638b

- 1
2
3 14. (a) Bergmann, L.; Hedley, G. J.; Baumann, T.; Bräse, S.; Samuel, I. D. W., Direct Observation of
4 Intersystem Crossing in a Thermally Activated Delayed Fluorescence Copper Complex in the Solid State.
5 *Science Advances* **2016**, *2* (1), e1500889, DOI: 10.1126/sciadv.1500889;
6 (b) Leitz, M. J.; Kühle, F.-R.; Mayer, H. A.; Wesemann, L.; Yersin, H., Brightly Blue and Green Emitting
7 Cu(I) Dimers for Singlet Harvesting in Oleds. *The Journal of Physical Chemistry A* **2013**, *117* (46), 11823-
8 11836, DOI: 10.1021/jp402975d;
9 (c) Krylova, V. A.; Djurovich, P. I.; Whited, M. T.; Thompson, M. E., Synthesis and Characterization of
10 Phosphorescent Three-Coordinate Cu(I)-Nhc Complexes. *Chemical Communications* **2010**, *46* (36), 6696-
11 6698, DOI: 10.1039/c0cc01864c
12
13
14 15. Lin, S.; Peng, Q.; Ou, Q.; Shuai, Z., Strong Solid-State Fluorescence Induced by Restriction of the
15 Coordinate Bond Bending in Two-Coordinate Copper(I)-Carbene Complexes. *Inorganic Chemistry* **2019**,
16 *58* (21), 14403-14409, DOI: 10.1021/acs.inorgchem.9b01705
17
18
19 16. (a) Herzberg, G.; Teller, E., Schwingungsstruktur Der Elektronenübergänge Bei Mehratomigen
20 Molekülen. In *Zeitschrift für Physikalische Chemie*, 1933; Vol. 21B, p 410;
21 (b) Renner, R., Zur Theorie Der Wechselwirkung Zwischen Elektronen- Und Kernbewegung Bei
22 Dreiatomigen, Stabförmigen Molekülen. *Zeitschrift für Physik* **1934**, *92* (3), 172-193, DOI:
23 10.1007/bf01350054;
24 (c) Merrill, W. A.; Stich, T. A.; Brynda, M.; Yeagle, G. J.; Fettingner, J. C.; De Hont, R.; Reiff, W. M.;
25 Schulz, C. E.; Britt, R. D.; Power, P. P., Direct Spectroscopic Observation of Large Quenching of First-
26 Order Orbital Angular Momentum with Bending in Monomeric, Two-Coordinate Fe(Ii) Primary Amido
27 Complexes and the Profound Magnetic Effects of the Absence of Jahn- and Renner-Teller Distortions in
28 Rigorously Linear Coordination. *Journal of the American Chemical Society* **2009**, *131* (35), 12693-12702,
29 DOI: 10.1021/ja903439t;
30 (d) Zadrozny, J. M.; Xiao, D. J.; Atanasov, M.; Long, G. J.; Grandjean, F.; Neese, F.; Long, J. R., Magnetic
31 Blocking in a Linear Iron(I) Complex. *Nature Chemistry* **2013**, *5*, 577, DOI: 10.1038/nchem.1630
32
33
34 17. Herzberg, G., *Molecular Spectra and Molecular Structure*. Krieger: Malabar Fla., 1991.
35
36
37 18. (a) Dance, Z. E. X.; Ahrens, M. J.; Vega, A. M.; Ricks, A. B.; McCamant, D. W.; Ratner, M. A.;
38 Wasielewski, M. R., Direct Observation of the Preference of Hole Transfer over Electron Transfer for
39 Radical Ion Pair Recombination in Donor-Bridge-Acceptor Molecules. *Journal of the American Chemical*
40 *Society* **2008**, *130* (3), 830-832, DOI: 10.1021/ja077386z;
41 (b) Pintaric, C.; Olivero, S.; Gimbert, Y.; Chavant, P. Y.; Duñach, E., An Opportunity for Mg-Catalyzed
42 Grignard-Type Reactions: Direct Coupling of Benzylic Halides with Pinacolborane with 10 Mol % of
43 Magnesium. *Journal of the American Chemical Society* **2010**, *132* (34), 11825-11827, DOI:
44 10.1021/ja1052973;
45 (c) Wiedbrauk, S.; Maerz, B.; Samoylova, E.; Reiner, A.; Trommer, F.; Mayer, P.; Zinth, W.; Dube, H.,
46 Twisted Hemithioindigo Photoswitches: Solvent Polarity Determines the Type of Light-Induced Rotations.
47 *Journal of the American Chemical Society* **2016**, *138* (37), 12219-12227, DOI: 10.1021/jacs.6b05981
48
49
50 19. Shao, Y.; Gan, Z.; Epifanovsky, E.; Gilbert, A. T. B.; Wormit, M.; Kussmann, J., et al., Advances in
51 Molecular Quantum Chemistry Contained in the Q-Chem 4 Program Package. *Molecular Physics* **2015**,
52 *113* (2), 184-215, DOI: 10.1080/00268976.2014.952696
53
54
55
56
57
58
59
60

- 1
2
3 20. (a) Grimme, S.; Antony, J.; Ehrlich, S.; Krieg, H., A Consistent and Accurate Ab Initio Parametrization
4 of Density Functional Dispersion Correction (Dft-D) for the 94 Elements H-Pu. *Journal of Chemical*
5 *Physics* **2010**, *132* (15), 19, DOI: 10.1063/1.3382344;
6 (b) Yanai, T.; Tew, D. P.; Handy, N. C., A New Hybrid Exchange–Correlation Functional Using the
7 Coulomb-Attenuating Method (Cam-B3lyp). *Chemical Physics Letters* **2004**, *393* (1), 51-57, DOI:
8 <https://doi.org/10.1016/j.cplett.2004.06.011>
9
10
11 21. (a) Partyka, D. V.; Zeller, M.; Hunter, A. D.; Gray, T. G., Relativistic Functional Groups: Aryl Carbon-
12 Gold Bond Formation by Selective Transmetalation of Boronic Acids. *Angewandte Chemie-International*
13 *Edition* **2006**, *45* (48), 8188-8191, DOI: 10.1002/anie.200603350;
14 (b) Gaillard, S.; Slawin, A. M. Z.; Nolan, S. P., A N-Heterocyclic Carbene Gold Hydroxide Complex: A
15 Golden Synthone. *Chemical Communications* **2010**, *46* (16), 2742-2744, DOI: 10.1039/c0cc00018c
16
17
18 22. Noviandri, I.; Brown, K. N.; Fleming, D. S.; Gulyas, P. T.; Lay, P. A.; Masters, A. F.; Phillips, L., The
19 Decamethylferrocenium/Decamethylferrocene Redox Couple: A Superior Redox Standard to the
20 Ferrocenium/Ferrocene Redox Couple for Studying Solvent Effects on the Thermodynamics of Electron
21 Transfer. *The Journal of Physical Chemistry B* **1999**, *103* (32), 6713-6722, DOI: 10.1021/jp991381+
22
23
24 23. (a) Jin, M.; Chung, T. S.; Seki, T.; Ito, H.; Garcia-Garibay, M. A., Phosphorescence Control Mediated
25 by Molecular Rotation and Auophilic Interactions in Amphidynamic Crystals of 1,4-Bis[Tri-(P-
26 Fluorophenyl)Phosphane-Gold(I)-Ethynyl]Benzene. *Journal of the American Chemical Society* **2017**, *139*
27 (49), 18115-18121, DOI: 10.1021/jacs.7b11316;
28 (b) Lin, S. H., Rate of Interconversion of Electronic and Vibrational Energy. *The Journal of Chemical*
29 *Physics* **1966**, *44* (10), 3759-3767, DOI: 10.1063/1.1726531;
30 (c) Schloman, W. W.; Morrison, H., Organic Photochemistry. 35. Structural Effects on the Nonradiative
31 Decay of Alkylbenzenes. The Nature of The ".Alpha.-Substitution Effect". *Journal of the American*
32 *Chemical Society* **1977**, *99* (10), 3342-3345, DOI: 10.1021/ja00452a025
33
34
35 24. Mierzejewska, K.; Bochtler, M.; Czapińska, H., On the Role of Steric Clashes in Methylation Control
36 of Restriction Endonuclease Activity. *Nucleic Acids Research* **2016**, *44* (1), 485-495, DOI:
37 10.1093/nar/gkv1341
38
39
40 25. (a) Freed, K. F.; Jortner, J., Multiphonon Processes in Nonradiative Decay of Large Molecules. *Journal*
41 *of Chemical Physics* **1970**, *52* (12), 6272-+, DOI: 10.1063/1.1672938;
42 (b) Englman, R.; Jortner, J., Energy Gap Law for Radiationless Transitions in Large Molecules. *Molecular*
43 *Physics* **1970**, *18* (2), 145-+, DOI: 10.1080/00268977000100171
44
45
46 26. Vogt, R. A.; Gray, T. G.; Crespo-Hernandez, C. E., Subpicosecond Intersystem Crossing in Mono- and
47 Di(Organophosphine)Gold(I) Naphthalene Derivatives in Solution. *Journal of the American Chemical*
48 *Society* **2012**, *134* (36), 14808-14817, DOI: 10.1021/ja303592q
49
50
51
52
53
54
55
56
57
58
59
60



By careful ligand design, excited state is shifted from MLCT to ICT with the elimination of Renner Teller distortion and bond rotation, enhancing photoluminescent quantum yield.